DEVELOPMENT OF MICROFLUIDIC PAPER BASED ANALTYICAL DEVICE (μ-PAD) USING 3D PRINTING FOR WOUND FLUID ANALYSIS

PRIYADARSINI S
(BT15M005)

A thesis submitted in partial fulfillment of the requirements

for the award of the degree

MASTER OF TECHNOLOGY, CLINICAL ENGINEERING

DEPARTMENT OF BIOTECHNOLOGY

INDIAN INSTITUTE OF TECHNOLOGY, MADRAS

DECEMBER 2017

THESIS CERTIFICATE

This is to certify that the thesis titled, **Development of microfluidic paper based analytical device (μ-PAD) using 3D printing for wound fluid analysis** submitted by **Priyadarsini S** (Reg No. BT15M005), to the Indian Institute of Technology Madras, Chennai for the award of the degree of **Master of Technology in Clinical Engineering**, is a bona fide record of the research work done by her under my supervision. The contents of this thesis, in full or in parts, have not been submitted to any other Institute or University for the award of any degree or diploma.

Dr. Lynda. V. Thomas
Research Guide
Scientist D
Dept. of Tissue Engineering and Regeneration Technologies
Biomedical Technology Wing
Sree Chitra Tirunal Institute of Medical Sciences
Trivandrum-695012

Place: Trivandrum

Date: 24th December 2017

ACKNOWLEDGEMENTS

The work completed in this dissertation would not have been possible without the assistance, advice, encouragement, and patience of many individuals. First and foremost, I am immensely grateful to my guide Dr. Lynda V. Thomas for giving me an opportunity and proper guidance to carry out my project at Department of Tissue Engineering and Regeneration Technologies, BMT Wing, SCTIMST and extending full-fledged support to me with enthusiasm to tackle various obstacles throughout the duration of the project. I would also like to thank Dr. Prabha D. Nair, Head of the Department of Applied Biology and Scientist in Charge, Department of Tissue Engineering and Regeneration Technologies, for giving me valuable suggestions and the opportunity to conduct my research at her lab providing all the facilities required for the smooth completion of my research work. I am also deeply grateful to the Director, SCTIMST, Dr. Asha Kishore, and Head, BMT Wing, Dr. Harikrishna Varma for extending all the facilities required for the smooth completion of my coursework and my dissertation. I express my sincere gratitude to Dr. Mukesh Doble, Dr. Suresh Devasahayam, Mr. Muraleedharan C. V. and Dr. Roy Joseph for coordinating the course and making this research a possibility.

My research endeavor would not have been complete without the support of many scientists and staff at the BMT campus. I am grateful to Mr. Muraleedharan C. V, Associate Head and Mrs. Leena Joseph of the Calibration cell who provided me the opportunity to conduct the Profilometric studies at their lab. I also would like to acknowledge the help rendered by Dr. Manoj Komath and Mr. Nishad K. V. for the SEM imaging. My sincere thanks to Dr. K. Harikrishna Bhat, Testing and Analytical Services Cell, NIIST, Trivandrum for helping me to conduct the BET analysis through their service facility. I would like to specially acknowledge the support provided by Mr. Vinod Kumar V., from the Division of Extracorporeal Devices and Swathi Designs, Trivandrum for helping me to fabricate the reader device which I could use for my study. I also would like to thank Mr. Anoop. G., Division of Artificial Internal Organs, for helping me to understand the concepts of simulation

and modeling on COMSOL software.

I would like to thank all my lab members and MTech classmates who were very supportive to carry out my research from the beginning. On a personal note, I would like to acknowledge every member of the Division of Tissue Engineering and Regeneration Technologies Laboratory where I completed my project, for their support during this work. I am extremely grateful to my family who relentlessly support me. Above all, I thank Almighty for the immense blessings he has showered on me.

Priyadarsini.S

ABSTRACT

In low-resource settings, where functional laboratories are not that developed, the potential of microfluidics can be exploited to deliver health care as a diagnostic device in a very cost effective and rapid manner. This work reports a novel, single step, cost effective fabrication technique for development of a paper based microfluidic analytical device (μPAD) and its characterization, which utilizes the syringe based system of a modified fused deposition modeling type 3D printer. The unique aspect of creating microfluidic paper analytical devices lies in the use of a hydrophobic patterning reagent to define hydrophilic flow channels for directing sample from an inlet to a defined location for subsequent analysis. In this study, 3D printing of polycaprolactone based ink (M_W 70000-90000) was employed for the generation of functional hydrophobic barriers on Whatman qualitative filter paper grade 1(thickness 180 μm and pore diameter 11 μm) which would effectively channelize fluid flow to multiple assay zones dedicated for different analyte detections. The presented work involves standardization, characterization and modeling of the 3D fabrication technique which improves the reproducibility and scalability, and preliminary studies on its application as a multi analyte quantification system for wound fluid implementing an android based colorimetric detection. The characterization studies reveal that a functional hydrophilic channel for sample conduction, fabricated using the reported technique can be as minimum as 460.7 μm and a functional hydrophobic barrier can be of any width with a lower limit of 866μm when a minimum of two layers of the suggested ink is extruded onto paper. A comparison with the hydrodynamical model established for writing with ink is used to explain the width of the line printed by this system. The presented fabrication technique proves to be a robust strategy that effectively taps the advantages of this 3D printing system in the production of μPADs with the characterization studies further exploring its employability in this realm with enhanced reproducibility. Preliminary studies on multi analyte quantification involved attempts to standardize and calibrate the concentration of glucose and pH of simulated wound fluid based on a colorimetric detection on the fabricated μPAD and employing an android application to read the result which would facilitate the same for the user. The studies show potential application of this microfluidic paper based system for wound fluid diagnostics.

TABLE OF CONTENTS

LIST OF TABLES…… 6

LIST OF FIGURES…… 7

ABBREVIATIONS…… 10

CHAPTER 1-INTRODUCTION…… 12

Origin of microfluidic analytical devices…… 12

Paper-based Microfluidics: New Tools for Point-of-Care diagnostics…….. 14

Paper based microfluidics, regulating flow parameters and characterization tests…… 17

Patterning of µPADs …… 19

Paper substrate used in µPADs …… 23

Use of 3D printing in POCs and PADs …… 24

Use of Poly(caprolactone) (PCL) as the ink in 3D printing…… 27

Sensing technologies as Diagnostic tools in PADs …… 28

Wound fluid analysis –Challenges and key considerations…… 31

Significance of study …… 36

Hypothesis…… 38

Objectives of study …… 38

CHAPTER 2 – MATERIALS AND METHODS…… 40

Choice of printing and imaging system …… 40

Choice of paper and ink…… 41

Standardization of print and printer settings …… 42

Modeling of printing…… 44

Fabrication process …… 46

Characterization of fabricated channel system…… 47

Fluid flow analysis in channels …… 47

Preliminary studies for two analyte detection 48
Glucose Estimation..... 48
pH Estimation 49
Imaging system..... 52
Algorithm of the developed android based application for detecting the colorimetric reaction 54
CHAPTER 3 – RESULTS AND DISCUSSION..... 56
Choice of ink and print settings 56
Modeling..... 59
Characterization of printing 63
Fluid flow analysis 65
Preliminary studies for two analyte detection..... 66
Glucose estimation..... .66
pH estimation 69
SUMMARY AND CONCLUSION..... 71
FUTURE PERSPECTIVES..... 72
REFERENCES..... 73

LIST OF TABLES

No.	Caption	Page
1	Table depicting the measured pH and the buffer systems used in the study	50
2	The viscosity of the different concentrations of PCL (w/v %) in chloroform	57
3	The print parameters that has been standardized for the printing process	59
4	The parametric results obtained for each of the parameters used in simulating the hydro dynamical model for comparison of the print width with the experimental printed width (mm). The hydrodynamically modeled width is calculated as per the equation, width, w=0.16η2h +5.55 R where η = (Φ/Ca)0.5, ϒ= surface tension of the ink, h = liquid film thickness, R = radius of nib opening, Φ = surface roughness, Ca, capillary number = μu0/ϒ, μ =viscosity of ink, u0= velocity of pen.	62
5	Table depicting the width of the printed lines on deposition on deposition of layers (4 to 10)	63
6	Table depicting the width of the printed line before and after heating while applying the backing support of PCL.	64
7	The value coordinates corresponding to the concentration of glucose in mM	68
8	The value coordinates corresponding to the pH.	70

LIST OF FIGURES

No.	Caption	Page
1	Different patterning methods of paper- Direct and Indirect	22
2	Wax patterning on paper by Whiteside's et al.	24
3	Currently used point of care diagnostic technologies	30
4	Illustration of the steps involved in the preparation and detection. Once the μPADs are developed, it involves the physical blotting method to input the required analytes (0.5 μl-2μl) in the test zone. After the time required for drying the blot, 3-6 μl samples may be introduced through the inlet zone. The third step involves the insertion of the μPAD, after the sample has reached the test zone, in the reader device which is attached to the smart phone and the fourth step involves capturing the image and reading the result using the developed app.	39
5	The 3D syringe based printer system (Makercity, Vandrum Technologies Pvt Ltd) used for developing the μPAD	41
6	Whatman Filter Paper Grade I, 150mm diameter which was used for the μPAD development process	42
7	a) Flow chart showing fabrication process of μPAD using 3D printed PCL microfluidic channels b) A representative image of a printed single channel μPAD tested using simulated thin wound fluid (C) Representation of a 3D printed paper cross section	46
8	Illustration of the pH based color change while using anthocyanin as the pH indicator	52
9	Black reader device which can be fixed onto the smartphone device. The device houses a slit on the top surface to introduce the μPAD and 2 LED lights illuminate the black reader box from either side. The LED lights are powered by the phone using microUSB OTG connection.	53
10	Algorithm of developed android based application for detecting the colorimetric reaction	54
11	Screen shots depicting control flow of the developed android application.	55
12	A) Standardization of PCL ink concentration by leak test, (1) 3%, (2) 5% and (3) 8%; B) Leakage test when using different needle diameters (1) 26 G, (2)24 G, (3)	57

	21 G	
13	SEM images showing the top and bottom surface of a fabricated µPAD	58
14	Representative image of the drop profile for measurement of surface tension using the pendant drop method in contact angle testing.	60
15	Calculation of the Surface roughness (a) from BET analysis, (b) BET surface area plot of Relative pressure (P/Po) against 1/[Q(P0/P-1]	61
16	Profilometric plot for calculating the liquid column height (h)	61
17	Plot of needle diameter, mm Vs width (mm). The linearity and correlation of the experimental width with the needle diameter is evident from this graph.	62
18	Design used for finding minimum hydrophilic channel width. Channel widths (1mm, 2mm, 2.5mm and 3mm) were explored in this study.	64
19	A representative image of (a)minimum hydrophilic channel and (b) minimum hydrophobic barrier width imaged under 5X objective of an optical microscope system. The image was analyzed using ImageJ software**.**	64
20	Figure showing the time taken by both rabbit blood plasma and simulated thin wound fluid to traverse the channel and reach the assay zone. Both the fluids were able to reach the test zone in 195 sec.	65
21	Graph depicting the distance moved in cm Vs the square root of time in sec.	66
22	Three channel systems with three assay zones used for glucose estimation where sample is introduced at center. Solid drawing was taken with an infill of 0% where the perimeters were only considered. The length of the channel between the inlet and assay zone was 1cm and the diameter of the test zone being around 5mm.	67
23	Graph showing the concentration of standard Glucose solutions in mM against the value coordinate (LoD = 3Mm, sensitivity = 0.66)	67
24	The blotted results of the different standard glucose solutions used to prepare the calibration curve. An unknown sample was also attempted to find the accuracy of the calibration done using 7mM/L Glucose solution.	68
25	Two channel systems used for pH estimation. Solid drawing was used with an	69

	infill of 0% where the perimeters were only considered. The length of the channel between the inlet and assay zone was 1cm and the diameter of the test zone being around 5mm.	
26	The initial blotted results (before full wet out) of the different standard pH solutions used to prepare the calibration curve. The color was in accordance with the pH color scale in the entry area of the assay zone with a pink corona which indicates the color of the control.	70

ABBREVIATIONS

2D	Two dimensional
3D	Three dimensional
µpad	Microfluidic paper analytical device
APTES	Aminopropyltriethoxy silane
CE	Capillary Electrophoresis
CL	Chemiluminescence
DARPA	Defense advanced research projects agency
ECL	Electrogenerated chemiluminescence
ELISA	Enzyme Linked Immunosorbent Assay
FDM	Fused Deposition Modelling
GPC	Gas phase chromatography
GOx	Glucose Oxidase
HPLC	High pressure liquid chromatography
HSV	Hue,Saturation,Value
LCD	Liquid crystal display
LFA	Lateral flow assay
LoD	Limit of detection
LSPR	Localized Surface Plasmon resonance
NCM	Nitrocellulose membrane
Np	Nano particle
OTS	Octadecyltrichlorosilane
PBS	Phosphate buffered saline
PCL	Polycaprolactone
PDMS	Polydimethoxysilane
PEC	Photoelectrochemical
POCT	Point of care testing
PSA	Prostate specific antigen
RGB	Red, Blue, Green
SEM	Scanning Electron Microscopy
SERS	Surface-enhanced Raman scattering
SIM	Simulated
SLA	Stereolithography
WHO	World Health Organization

CHAPTER 1 - INTRODUCTION

Origin of microfluidic analytical devices

In 1938, Ukrainian scientists N.A. lzmailov and his student M.S. Shraiber worked on Spot chromatographic method of analysis for plant extracts (1). They coated microscope slides with a suspension of various adsorbents (calcium, magnesium, and aluminum oxide), deposited one drop of the sample solution on this layer and added one drop of the solvent. The sample components which were separated appeared as concentric rings that fluoresced in various colors under a UV lamp (2). This marked the beginning of microfluidics. The application of microfluidic analytical devices is spread across four major domains which are molecular analysis, bio-defense, molecular biology and microelectronics. The origin of microfluidic microanalytical methods can be traced back to the invention of analytical methods like Gas Phase Chromatography (GPC), High Pressure Liquid Chromatography (HPLC) and Capillary Electrophoresis (CE), which have revolutionized chemical analysis. The first real lab-on-a-chip was created in 1979 at Stanford University for gas chromatography. The incorporation of optical detection techniques using LASER has further enhanced miniaturization by reducing the sample volume required and improving accuracy (3). This was followed by exploration of versatile microanalytical techniques for analysis.

In 1990's after the end of the cold war, chemical and biological weapons posed major military and terrorist threats. For the development of detectors to overcome these threats, the Defense Advanced Research Projects Agency (DARPA) of the US Department of Defense supported a series of programs aimed at developing field-deployable microfluidic systems designed to serve as detectors for chemical and biological threats. This led to the rapid growth of microfluidic technology. The 1980s saw the advent of high throughput genomic techniques and other areas of microanalysis related to molecular biology, which required analytical methods with enhanced sensitivity and resolution which can be met by employing microfluidic technologies, apart from being used in inkjet print heads, micro propulsion and micro-thermal technologies. These advances miniaturized operations to the level of a single cell for the first time. In the 90's microelectronics also stimulated the growth of microfluidics and investigated its application in biology, chemistry and biomedical fields. Silicon and glass based fluidic microsystems in the earlier part of the era which required heavy infrastructure and electronics was replaced by plastics. At this point majority of focus was on integrating the various chemical, biological and biomedical protocols onto a single chip. Such systems enabled the implementation of the complete protocol beginning with sample collection up to analysis and are called micro total analysis systems (4). In the early 2000s, the technique of fabricating such micro-channels using polymers such as PDMS was highly preferred since it reduced the production time and cost effectively. These were generally known as soft-lithography techniques (5).

In 2004, POCKET, a portable microfluidic-based system was introduced by Whiteside's group which addressed the requirements of simple diagnostic devices in developing countries (6). POCKET was used for carrying out immunoassays with the same efficiency as bench-top ELISA, but in a lesser time in a cost-effective manner (7). Conventional microfluidic devices seemed to be too complicated and expensive to be used on a large scale in developing countries which marked a shift towards paper based microfluidics, which are widely referred to as paper based analytical devices (PADS). The concept of micro pads (μPADs) was described by Whiteside's Group of Harvard University in 2007 (8). A similar technique was used in the past around 1940s by Müller and Clegg, apart from the use of paper strips for pH determination. They created wax barriers on filter paper and observed that the restricted channel resulted in reduced sample consumption with its quick diffusion process, and achieved separation in the order of magnitude of micrograms (9). In recent years, μPAD technologies are finding wide range of applications in health diagnostics, biochemical analysis, forensic and food and environment quality control (10).

Paper based microfluidics (μ-PAD): New tools for point of care diagnostics

μPADs are very small, inexpensive, easy to use and can be used as modes of quantitative detection while used with commonly available smart phone cameras. Paper has been used as a substrate material in analytical testing for centuries, since the use of litmus paper began in 1800s. The potential of using paper as a substrate in analyte detection has been explored in 1930s to build multiwelled assay plates and fluidic systems for chemical

analysis (11, 12). In around 1950s, the first semi quantitative glucose paper based diagnostic device for estimating glucose levels in urine was conducted (13). This was further extended to paper based immunological test devices (ELISA kits) and has been commercialized as NCM based dipsticks in 1982 (14, 15). Lateral flow was introduced to these dipsticks which eliminated incubation and washing steps involved in the use of dipstick technology (16). These technologies highly improved specificity, range of detectable analytes while achieving higher LoDs (Limit of detection). Since the work of Whiteside's group was published in 2007, the interest towards development of µPADs was renewed (17-21). The most important step in the fabrication of a µ PAD is the creation of hydrophobic barriers on paper which can be patterned into hydrophilic channels that effectively wick the sample fluid to the different assay zones. The preliminary attempt to fabricate a PAD involved stamping patterns of Scotch guard on paper which failed to produce PADs with dimensional accuracy. Later photolithography emerged as a successful patterning method for PADs and this led to the introduction of first µPAD in 2007. Currently the available methods for patterning paper are: photolithography, plotting, inkjet printing, plasma etching, flexographic printing (22), wax printing and cutting patterns of channels from a sheet of paper (23). Even though µPADs have not been as successful as POCKET, recently developed paper based ELISA represents a step towards it. The applications of µPADs have been demonstrated by conducting colorimetric assays for several analytes including glucose, bovine serum albumin, nitrites, ketones, alkaline phosphatase and cholesterol (24). Other methods of detection including electrochemical (24), transmittance (25), chemiluminescence (26) and fluorescence.

According to WHO guidelines, low-cost sensors which could serve as POCTs in resource-limited settings was defined to comply as “ASSURED” that is “affordable, sensitive, specific, user-friendly, rapid and robust, equipment-free and delivered to those in need” which is concomitant with µPADs (28). More research is now carried out in enhancing the user friendliness and longevity of these POCTs.

µPADs find applications in many areas like clinical monitoring, diagnosis (28,29,8,30), veterinary (31), food industry (32-34), agriculture (35,36,37) and environmental safety (38-40). They have also been employed in detecting a range of analytes like biomarkers (28,29,8,30), drugs (35,41,42,43), protein (8,44), hormones (45,46), bacteria (39,45,48-50), viruses (51-54), contaminants (37,70), toxins (64,66,67), heavy metals (68,69,41,70,71), also analyte capturing can be brought about by immobilising any reagents from enzymes(8,55) to functional DNA (44,67,72) molecules such as aptamers. Many methods are used to immobilise reagents on µPADs like physical absorption, chemical coupling, carrier-mediated (via nanoparticles) deposition, sol gel processing, dip casting, contact and non-contact inkjet printing (73,74). Different nano particles like AuNP, AgNP, liposomes were used to improve sensitivity (42,70,75,76). µPADs has also been modified to include sample pre-treatment procedures like plasma separation from whole blood by using serum separation membrane as demonstrated by Pollock et al, by introducing blood grouping antibodies which worked for antibody positive RBCs (78,79) , by using salt solutions as by Nilghaz et al (80). Noiphung et al (81) introduced the concept of electrochemical paper device which used plasma isolation units which comprised of

Whatman VF blood separation paper. These efforts reduced the pre-treatment steps to a considerable level.

Paper based microfluidics - Regulating the flow parameters and characterisation tests

Microfluidic platforms are of five major types based on the liquid propulsion system which are capillary, pressure driven, centrifugal, electrokinetic and acoustic systems. Cellulose paper is a porous material composed of fibre networks with average fiber diameter of 1–100 μm, and pore space with average pore size of 1–10 μm. Capillarity is the major mechanism of flow in cellulose paper. Paper being hydrophilic provides a low contact angle and adhesive forces while the surface tension of the liquid tries to reduce the liquid gas interface area which helps in rapid wicking. This leads to capillary flow and the flow is sustained by the pressure difference between the wet and relatively dry area. Wicking in cellulose paper is usually predicted and analyzed using two different models: 1) the Lucas–Washburn equation derived from the Hagen–Poiseuille law where the pores in the medium are considered as isotropic capillary tubes, and 2) Darcy's law. The micro pores of cellulose paper results in Reynolds numbers (ρvd/μ) lower than 1, where ρ is the fluid density (kg/m³), V is the fluid velocity (m /s), δ is the characteristic pore size (m) and μ is the fluid dynamic viscosity (Pa. s) which renders the flow laminar where the viscous forces are dominant. Equilibrium between surface tension and viscous forces characterizes the

velocity of flow. Darcy's law can be applied in this case for analyzing flow of Newtonian fluids (constant density and viscosity)

$$Q = -AK\Delta h/L$$

where *Q* is volumetric flow rate (m3/s), A is the flow area perpendicular to L (m2), K is the hydraulic conductivity (m/s), h is the hydraulic head or height (m), which is the sum of the pressure head (P) and the elevation (z); L is the flow path length(m). The hydraulic head decreases in the direction of flow i.e. from a region of high pressure to a region of low pressure which is indicated by negative sign. The hydraulic conductivity (K) is the proportionality coefficient and is a function of both the permeability of the medium and the fluid properties the pressure is lower. The distance moved by the liquid front (L) during the wetting process in the paper strip can also be estimated using the Washburn Equation (82).

$$L^2 = \gamma D t/2\mu$$

where L is distance traveled by the liquid front within the porous material (paper) whose pore diameter is D, *t* is time, γ and m are respectively the surface tension and viscosity of the liquid. According to this equation, the distance traveled by the liquid is directly proportional to surface tension of the liquid and inversely proportional to viscous resistance. This is widely applied in case of one dimensional fluid wet out. The multiple

approximations (pore size, geometry and distribution, constant porosity and permeability) and assumptions (perfectly wetting liquid, non-limiting source, negligible swelling effect, and flow through interconnected pore channels) used to calculate the parameters of interest which may lead to some deviations. Most of the research and modeling performed today on paper microfluidics use the either of the two models or its modified versions. Schuchardt and Berg proposed a modified equation based on fiber swelling that the pore radius in the wetted area of a porous medium such as cellulose paper will decrease linearly with time because of wicking and fiber swelling (83). In three dimensional PADs, Washburn model is modified to include gravity term. Channel geometries have also been studied to improve pretreatment efficiency of the sample. Yager et al. established a relationship between flow transport time and the channel width (84). This is a very important finding which would help in the controlled delivery of reagents to the reaction zone by adjusting the strip width (85).

Patterning of µPADs -Advantages and limitations

Any biosensor development involves the integration of three important components: a fluid handling system, a transducer capable of converting one form of energy to another, and surface functionalization for sample pre – treatment or specific receptor – ligand interaction, so does the µ PADs. Paper-based microfluidics provide a non-suction flow by generating fluid transport through capillarity (41,60), unlike conventional microfluidic devices where the flow is pressure-driven using pumps, automated valves or pneumatic control systems. Microfluidic paper-based analytical devices can be fabricated either two

dimensionally (86,87,88) or three dimensionally (94,8,89,90,91,92,93) depending on the intended complexity. Hydrophobic patterning is the key to design of a µPAD. The two parallel hydrophobic lines form channels, because hydrophobic barrier retains the sample solution within the channel and consequently the liquid flows in the channels owing to capillary action. The wax-patterning method (97, 96, 95) has following merits; simple fabrication, it is rapid (5–10min), inexpensive (both wax and paper are cheap and easy to obtain), and environmentally friendly. Inkjet printing has also proven to be successful whose efficiency is determined by paper chemistry and inkjet printing technologies (98). Photolithography and flexographic printing are also simple methods for the fabrication of µPADs. In flexographic printing, polystyrene is printed flexographically to form liquid guiding boundaries and layers on paper substrates (99). Fabrication of the µPADs via plasma treatment is done as follows: Paper is firstly completely hydrophobized via octadecyltrichlorosilane (OTS) silanization and then the OTS silanized paper is subjected to plasma treatment using a mask which is designed according to the required channel geometry. The area of the paper exposed to plasma forms the hydrophilic channel network due to degradation of OTS molecules coupled to the paper's cellulose fibers before (100). Another method of fabrication is using laser-assisted polymerization of a photopolymer that has successfully guided the flow of fluids without any leakage. For fabrication by wet etching, as in plasma treatment method, paper is hydrophobized by trimethoxy octadecylsilane which is treated with a paper mask penetrated with sodium hydroxide solution (30% glycerol) with simultaneous etching of the salinized paper (101). Wax screen-printing consists of two simple steps that is: (1) printing patterns of solid wax on the

surface of paper using a simple screen-printer and (2) melting the wax deposited in paper to form complete hydrophobic barriers using a hot plate.

Trinh Lam et al. came up with chemically modified µPAD in 2017 by forming hydrophobic barriers using chemical vapor deposition of trichlorosilane on chromatography paper. They optimized various parameters like temperature, pattern size, and duration of deposition to characterize the spreading patterns, flow behavior and and hydrophobicity of patterns of different sizes. They also demonstrated glucose assay, immunoassay and heavy metal detection on the developed µPAD.

3D paper-based microfluidic devices are patterned in ways that channel the flow of fluid within and between layers of paper. They are fabricated by stacking alternating layers of paper and water impermeable double-sided adhesive tape (8). The hydrophobic polymer patterned in to the paper demarcates the channels through which the fluids move laterally, and the layers of water-impermeable double-sided tape separates the channels in the neighboring layers of paper and channelize the vertical flow of fluids in between the layers (8). In microchannel patterning, to direct liquid flow on paper devices, the paper needs to be patterned into hydrophilic channels separated by hydrophobic walls.

Depending on practical functional applications such as transport, mixing and detection, various methods have been developed to control fluid flow in paper-based biosensors. The immobilization of biomolecules that have usually an overall negative charge or citrate

capped nanoparticles require the use of cross linkers or intermediate surface coating. Three of the most commonly used approaches for the immobilization of the biomolecules are adsorption, covalent modification, and entrapment. Any application for sensing requires the integration with a transducer which could be colorimetric, electro – chemical or other materials capable of giving a measurable signal from the chemical reaction that occurs on the paper. The most cost-effective detection method is visual and colorimetric.

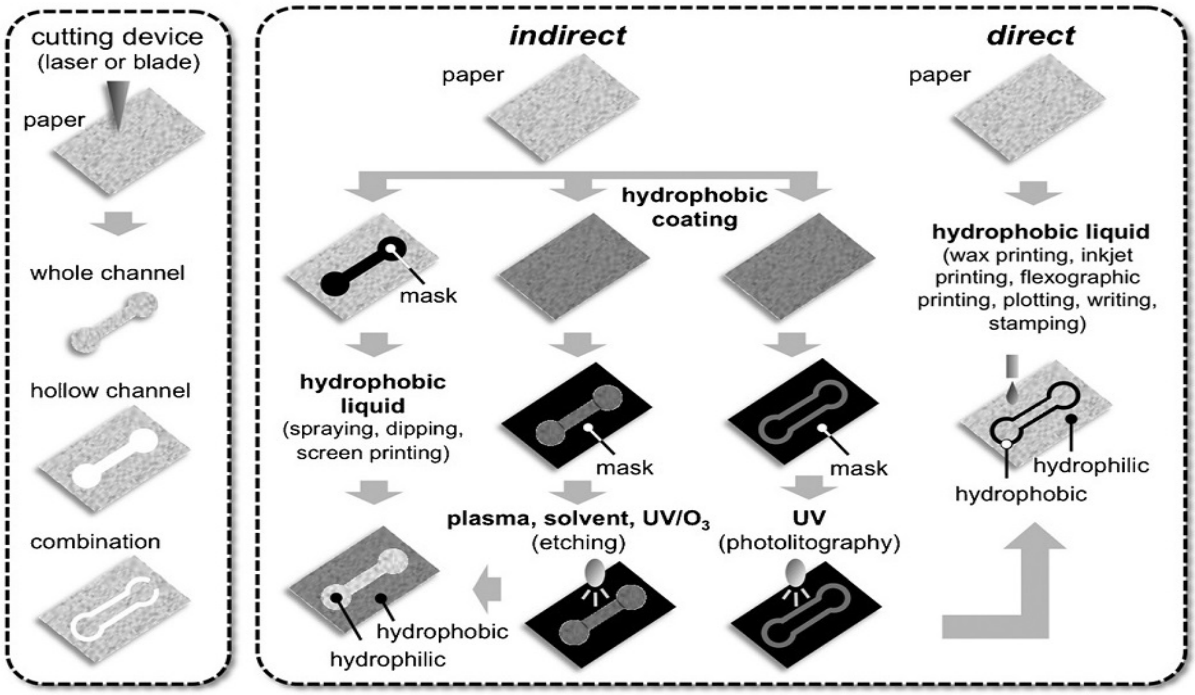

Figure 1: Different patterning methods of paper - Direct and Indirect.

Paper substrate used in µPADs

As the most abundant biopolymer on the Earth, cellulose is the major source of paper production industrially. Cellulose paper is a homopolymer of (1- 4)-β-glucopyranose linked through acetal bonds and forming long β-1,4-glucanchains. The hydroxyl groups of the chains make the paper hydrophilic with a negative charge. The different grades of cchromatography and filter paper gained a lot of attention in the development of paper based microfluidics. Printing paper became a less preferred choice due to the low porosity and surface tension effects (102). A high porosity substrate is also less preferred, as it may lead to the uncontrolled flow of the hydrophilization materials. For example, filter papers with larger pore sizes than the standard grade can swell their cellulose fibres and constrain the capillary flow. Sensitivity, specificity and reproducibility of the tests carried out greatly depend on the surface area of the substrate. When other parameters are kept constant, the surface area declines non-linearly with pore size, increases non-linearly with porosity and increases linearly with thickness (103).

Paper as a substrate has many unique advantages over traditional device materials including power-free fluid transport via capillary action, a high surface area to volume ratio that improves detection limits for colorimetric methods, cost effective and portable and can store reagents inactive form within the fibre network. Because of these benefits, paper is being used in a wide arena ranging from spot tests for metals (104) and paper chromatography (105) to lateral flow immunoassays. The natural porous microstructure of

paper, is amenable to lateral flow via capillary action, and hence helps in onsite analysis without the use of pumps (85,106-111). The normally used papers for patterning of hydrophilic channels are Whatman filter paper grade 1,3,4 (112) and nitrocellulose membranes. Of all, Whatman filter paper grade 1 has shown good uniformity and sensitivity for colorimetric detection (107). Paper towels available for domestic use is also experimented for use in PADs but proves to exhibit lower dimensional accuracy.

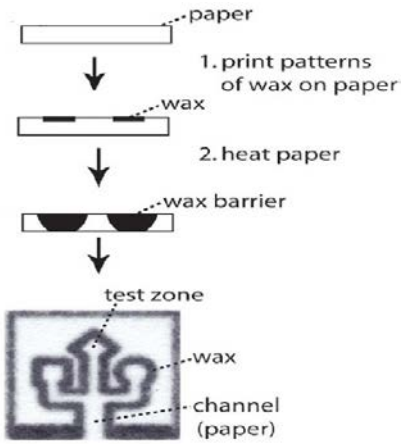

Figure 2 : Wax patterning on paper substrate by Whiteside's et al.

Use of 3D printing in POCs and PADs

Three-dimensional (3D) printing has been in use since a long time in the manufacturing sector to produce design prototypes (113), however the use of 3D printing to produce a completely functional device, such as tissue growth scaffolds, electronics, microfluidics and pneumatics have gained a lot of popularity recently (114-116). In 2012, Kitson et al had reported the use of 3D printing to initiate chemical reactions by printing reagents directly into a 3D 'reactionware' matrix (reactionware refers to devices that combine both reactor and reagent) (117). They successfully fabricated robust reactionware devices to carry out

chemical synthesis in a very rapid and cost-effective manner using 3D printing. They designed the devices using a freely distributed 3D Computer Aided Design (CAD) software package (Autodesk123D) and printed it with polypropylene (PP) using a 3DTouchTM printer which deposits layers of thermopolymers through heated extruder nozzles to build up the desired 3D architectures (118). Recently in 2017, Zongjie Wang et al demonstrated the capability of SLA printers for a specific resin for which they employed a liquid crystal display (LCD)-based SLA 3D printer for demonstrating its feasibility and applied optimized parameters for fabricating multilayer 3D microfluidic devices. It has been found that the LCD-based SLA 3D printer can be used for fabrication of microfluidic devices with a resolution of 400µm in the horizontal plane and 800µm in the vertical plane for interconnection features. They also standardised the curing time for different resins used for fabrication (119). Another group in 2017, Salentijn et al came up with microfluidic analytical devices fabricated by fused deposition modelling (120). For a benchtop FDM 3D printer, they characterized the requirements which include parameters like resolution, surface roughness, leakage, transparency, material deformation, possibilities for integration of other materials, the auto fluorescence, solvent compatibility, and biocompatibility of twelve representative FDM materials. This work thus provides a guideline for (i) the use of FDM technology by addressing its possibilities and current limitations, (ii) material selection for FDM, based on solvent compatibility and biocompatibility, and (iii) application of FDM technology to (bio) analytical research by demonstrating a broad range of illustrative examples. They have also demonstrated the use of FDM to create hydrophobic molds like wax patterns used for patterning hydrophilic

channels on paper. The 3D printed features are supposed to have the same dimensions as input in the CAD design which enables the fabrication of more sophisticated functional features compared to the other methods. Several functional parts of microfluidic devices like connection ports, flow regulating components, and integrated detectors can be fabricated using 3D printing. 3D printing can also be used in the production of personalized devices like dental implants, hearing aid (119). Most of the reported 3D-printed microfluidic devices have channel sizes from hundreds of microns to a few millimeters; lowest being 200µm channel (121) hence restrains its use in small channel applications like single cell channeling. Further limitations like biocompatibility, cost of high resolution 3D printers, surface finish also affect the preference towards 3D printers for fabricating microfluidic devices. YongHe et al in 2016 produced 3D printed PADs, printed by a desktop three-dimensional 3D printer, wherein the sample flow was driven by the capillary force of cellulose powder. In the method, a suitable size-scale substrate with open microchannels on its surface was printed. The surface of the device was covered with PDMS to seal the microgaps. Then, the microchannels were filled with a mixture of cellulose powder and deionized water in an appropriate proportion and dried at 60 °C for 30 minutes. A series of microfluidicanalytical experiments, including quantitative analysis of nitrite ion were also demonstrated (122). Multi material deposition can also be achieved by material jetting mode of 3D printing. An earlier attempt to model 3D printing was by Kyle Christensen et al where they studied the mechanism of layer formation in inkjet 3D printer. In 3D inkjet printing, droplets are ejected from a nozzle and each layer is formed droplet by droplet. In their study they have tried to elucidate the layer formation mechanism in terms of

formation of single lines and layers comprised of adjacent lines during drop-on-demand inkjet printing of alginate using high speed imaging and particle image velocimetry. The effects of printing conditions on the behavior of droplets during layer formation were modeled based on gelation dynamics, and recommendations were presented to enable controllable and reliable fabrication of gel structures (123).

Use of Poly(caprolactone) (PCL) as the ink in 3D printing

PCL, is a semi-crystalline and hydrophobic biodegradable polymer, which resists random hydrolytic chain scission of the ester groups and consequently degrades over a relatively long degradation period compared to other bioresorbable polymers. The use of PCL for the fabrication of scaffolds in tissue engineering has been explored already (124).PCL has previously been investigated for additive manufacturing applications (27,125-127), using Fused Deposition Modeling (FDM). Yinfeng He et al has characterized the behavior of solvent based PCL for material jetting (124). An initial study of material jetting of PCL was conducted using a Fujifilm Dimatix DMP-2830 material printer. This study explores a potential solvent based method of jetting polycaprolactone. Several solvents were used to prepare a PCL solvent based ink like ethanol, ethyl acetate, chloroform and 1,4-dioxane and out of this, chloroform and 1,4-dioxane gave positive results. Multi-layer PCL structures were printed and characterized. This work shows that biodegradable polycaprolactone can be processed through material jetting. To jet PCL, it is necessary to prepare it into a state where the key rheological parameters fall within those that allow printing. This group worked to establish the characterization of PCL jetting, determining appropriate solvents and set of printing

parameters that will afford jetting PCL and hence explores the potential of PCL in additive manufacturing.

Sensing technologies as diagnostic tools in PADs

Any application for sensing requires the integration with a transducer which could be colorimetric, electrochemical or other modes. Visual color formation is the most cost-effective method. The color shift in the visible range can be produced by many different phenomena and many types of reactions can be used for the development of colorimetric sensors (129). Continuous metal wires or thin films are used on a transparent substrate (130), or in localized mode known as localized surface Plasmon resonance (LSPR) which is majorly used on paper since it is fibrous and opaque, which requires the use of noble metal nanoparticles. These sensors exploit LSPR properties: Plasmonic colorimetry & Surface-enhanced Raman scattering (SERS). Electrochemistry is the second most used transduction system after colorimetry for μPADs. Planar electrodes are deposited on a paper substrate for detection of electrogenic reactions. This mode of detection also facilitates rapid, robust and miniaturized readers. Paper based biochemical detection has been employed to test many analytes. The signal resulting from the chemical reaction between sample and the immobilized reagent can then be detected by colorimetric, electrochemical, fluorescent, chemiluminescence (CL), Electrochemiluminiscence (ECL), or photoelectrochemical (PEC) methods (Ge etal.,2013). Immunoassay technique utilizes immunological detection for multiple applications, such as human chorionic gonadotropin (Apilux etal.,2013; Schonhorn etal.,2014), Escherichia coli O157:H7 (Reinholtetal.,2014), Rabbit IgG (Gerbersetal., 2014),

goat anti-rabbit IgG (Bai etal.,2013), and red blood cells agglutination.

Other detection methods that have been researched upon are calorimetric method for glucose determination (131), spectrophotometric method for phosphate and food dyes determination (132), mass spectrometry for acetylcholine hydrolysis determination (133), rhodamine 6G and L-phenylalanine determination, potentiometric methods metal ions determination, pH, polyvinyl amine and potassium polyvinyl sulfate determination. All these methods provide new platforms for diagnosis of diseases. Chemiluminescence based sensors detects the light intensity generated by a chemical reaction. Reagents are generally inexpensive, and give a highly sensitive measurement. Photo chemiluminescence (PL), a subset technique of chemiluminescence, Zhou et al used resonant energy transfer associated with upconverting phosphors. Electrogenerated chemiluminescence (ECL) is a variant of chemiluminescence which uses electrochemical reactions to generate luminescence. ECL offers low background optical signals, and provides better control over electrode potential and reagent addition, and selectivity is enhanced by controlling electrode potential (134).

Many colorimetric methods have been developed for glucose as it is an important biochemical analyte using either glucose oxidase (GOx) or GOx in combination with enzymes like horseradish peroxidise (HRP). For example, used tree-shaped µPADS with 2,4,6-tribromo-3-hydroxy benzoic acid and 4-aminoantipyrine to detect glucose. Protein and DNA-based biomarkers detection is another emerging area of research in point-of-care monitoring. Zhou et al. detected hydrogen peroxide using 3- aminopropyltriethoxysilane

(APTES) cross-linked with glutaraldehyde as a colorimetric reagent. The presence of H_2O_2 made the cross-linked APTES colorless. Anti-PSA immobilized on paper captured PSA and labeled with GOx-modified gold nanorods was used to detect PSA specific antigens (134).

The "color bar code" device developed by Lieberman's group for testing active pharmaceutical ingredients in antituberculosis drugs also utilizes colorimetric mode of detection (135). Similarly, Koesdjojo et al. developed a test for the counterfeit antimalarial drug Artesunate. Nanoparticles (NPs) are popular in cellulose and NCM based detection because they tend to be more stable than organic molecules and typically have higher extinction coefficients, consequently leading to better sensitivity for target analytes (137).

Figure 3: Currently used point of care diagnostic technologies.

Wound fluid analysis-Challenges and key considerations

Wound is transitional tissue that occurs due to any break in skin anatomy. Wound fluid is easily accessible and indicative of the status of wound healing and hence apart from clinical examination and microbiological swabbing, wound fluid analysis opens a scope for examination of wound microenvironment (138). A lot of interactions occur during wound healing and hence can be considered as a continuous and dynamic process. In general, wound healing during an acute injury constitutes of four main phases: - 1) conjugation 2) an early inflammatory phase 3) a late inflammatory phase 4) proliferative phase ending with remodelling and tissue restitution. Analysis of biochemical markers provides a better idea of progress in wound healing than systemic markers as they mostly do not exhibit tissue specificity. In diabetic foot, the analysis of biochemical markers might be of great clinical value and helps in predicting the probability of wound healing which assist the clinicians to arrive at conclusions during treatment which is vital as infection is a major cause of diabetes-related morbidity and mortality (138) and as it paves the way towards limb amputation (139). In this scenario, novel diagnostic tools that support prompt decision-making are urgently needed. Wound fluid consists of an inhomogeneous mixture of exudates and substances from blood whose composition is affected by many physiological conditions like cardiac failure or hydration status as well as vasoconstriction or diabetes. Ideally, wound fluid should be collected non-invasively with little effort, resulting in a better patient as well as greater physician acceptance.

Types of Wound Healing

Different categories of wound healing are primary intention, secondary intention or delayed primary intention. Primary healing occurs in the case of wounds that are just sutured and follows a non-infected healing method which requires minimum connective tissue deposition and epidermal cell migration to fill and cover the area of tissue loss, respectively. Secondary intention healing occurs when the wound is large where more of connective tissue deposition is required and significantly differ in the time for healing as it is susceptible to more infections. Cutaneous wounds that do not destroy sub epidermal appendages, such as the pilosebaceous unit, will epithelialize rapidly due to the store of epidermal cells present in these appendages from where they migrate out and cover the area. With wounds involving greater depth of the dermal connective tissue loss, epithelial cells must migrate from the wound edges, connective tissue must be deposited in greater volumes and the process of wound contraction may be required. Delayed primary healing is when primary closure is predicted to be unsuccessful, possibly due to the presence of infection, an inadequate blood supply, or the requirement of excessive tension during wound closure. In this case, at approximately three to five days, wound is undressed, and the edges are sutured closed as in primary intention closure. The rationale for this method of closure is to optimise the inflammatory response, increase angiogenesis at the wound edges and encourage natural decontamination of the wound. Normal wound healing involves successful completion of four overlapping phases conceptually defined as haemostasis, inflammation, proliferation, and remodelling, and commences the moment the injury to the tissue occurs. The initial injury results in an outflow of blood and lymphatic fluid activating both intrinsic and extrinsic clotting mechanisms.

Continuous wound measurement can be used to find wound healing probabilities and can find the cases that require more aggressive treatments. Wound assessments are generally conducted based on clinical experience relying on very basic equipment's to make objective measurements. Traditional methods of wound assessment, simple linear measurements, and wound tracings which are based on subjective interpretation of the wound and can lead to biased results. Therefore, it is important that measuring techniques with validity, accuracy, reliability, reproducibility, cost effectiveness and usability must be used.

There are several markers which are thought of as possible diagnostic and there are diagnostic targets. Some of the potential markers for wound healing as per Harding et al include

- Bacterial load/specific microbial species/biofilms
- Enzymes and their substrates – e.g. matrix metalloproteinases and extracellular matrix
- Exposed bone
- Growth factors and hormones – e.g. platelet-derived growth factor (PDGF), sex steroids (androgens/oestrogens), thyr oid hormones
- Immunohistochemically markers
- Inflammatory mediators – e.g. cytokines and interleukins
- Nitric oxide

- Nutritional factors – e.g. zinc, glutamine, vitamins
- pH of wound fluid
- Reactive oxygen species
- Temperature
- Trans epidermal water loss from peri wound skin

The surface of intact skin has a naturally acidic pH ranging from 4 to 6 due to organic secretion of keratinocytes. The secretions from sebaceous and sweat glands which include various acids, such as amino acids, lactic acid, and fatty acids also contribute to acidic pH, the acid mantle of the skin forms a defence against pathogenic microorganisms. The pH of the tissue underlying the skin is more neutral, around 7.4. During the initial stages of healing, the generation of organic acids leads to a temporary acidosis which is favourable for inducing proliferation of fibroblasts, promoting epithelization and angiogenesis, controlling bacterial colonization (Jones et al. 2015) and facilitating the release of oxygen from oxyhaemoglobin. Whereas, alkalinity can have an adverse effect on the wound tissue by depriving the wounds of oxygen which provides more favourable for bacterial growth. Hence pH is an important parameter for biochemical analysis of wound fluid. Generally non-healing wound shave been reported to have pH in the range of pH 7.15 to 8.93 (Gethin 2007) and it is at this stage that synthesis of extracellular molecules is impaired, and the healing process is stalled (Jones et al. 2015). As the wound advances through the process of healing, the pH moves to neutral and eventually returns to acidic (Schneider et al.2007, Percival et al. 2014a). In addition, bicarbonate and glucose levels increase in wound fluid during healing. Glucose levels remain low probably due to neutrophil

utilization as energy source. Hence glucose can also be considered as another important biochemical analyte for analysis. When a person has high glucose levels, they may have trouble healing from wounds. This happens as an increased amount of sugar in the blood causes the cell walls to become stiff and rigid, impairing the flow of blood throughout the small vessels located at the surface of the wound. As a result, it impedes the flow and permeability of red blood cells, which are required for the development of dermal tissue. Another way that high glucose levels affect the wound healing process is by impairing the hemoglobin release of oxygen. By doing so, it effectively starves the affected area of oxygen and nutrients that promote healing.

SIGNIFICANCE OF THE STUDY

In recent years, low cost point of care devices has been gaining popularity especially in the developing countries where access to laboratory testing in remote areas is limited. Point of care (POC) testing proves advantageous to the traditional diagnostic testing in clinical laboratory settings wherein timely information is provided to the clinicians who can take immediate decisions regarding diagnosis and treatment of infected and chronic wounds. Thus, the delay in sending samples to laboratory for testing and collection of results is prevented. Most of the point of care devices make use of microfluidics as their technology as it involves only small sample volumes leading to increased efficiency of chemical reagents, lower production and scale up costs, the ability to conduct high-throughput screening of biological targets; parallel processing of samples; fast sampling times; accurate and precise control of multiple samples and reagents simultaneously, thereby reducing the need for pipetting; low power consumption; and versatile format for the incorporation of various detection schemes, thereby leading to increased sensitivity. Colorimetry is the most used detection technique which can be easily read. In this context the advent of paper microfluidics is an innovative example which was developed as a low-cost technique which first emerged in 2007 with the goal of meeting the diagnostic accessibility in developing countries. The paper-based microfluidic diagnostics first emerged in 2007 as a low-cost alternative to conventional laboratory testing, with the goal of improving accessibility to medical diagnostics in developing countries. The advantages of the use of paper in microfluidic design are that it is biocompatible and can be easily disposed of and is compatible with various biological assays. The sample is usually capillary driven, and a wide range of colorimetric tests can be conducted

which can be easily detected qualitatively through the naked eye or quantified using imaging techniques which may be integrated in digital systems like cellular phones. This point of care diagnostic PAD will be useful in several developing countries and in remote settings where access to testing services is limited.

Our major challenge is therefore to develop such a multi-marker detection system in the form of a paper based microfluidic device, as a diagnostic tool to help classify the state of the wound, by detecting markers such as pH and glucose.

HYPOTHESIS

To develop a microfluidic paper based analytical device using 3D additive manufacturing technology for use in Point of Care (POC) analysis and multi-parameter based diagnosis of low volumes of wound exudates for wound management

OBJECTIVES OF STUDY

- Standardization of print settings in 3d printer for developing three channeled microfluidic system on paper and to develop two, three and four channel system using 3D printing technology. The 3D printing will be done using hydrophobic PCL polymer of different concentrations and the printing efficiency evaluated by varying different printing parameters. A backing support of PCL is to be provided for enhanced support.
- Modelling of printing procedure. To identify the parameters that affect the printed width on our substrate while using the syringe module of a fused deposition modelling type 3D printer and to predict an appropriate model to study the effect of using different needle gauge on the printed line width, the process of printing of a single layer will be compared to writing with ink on a paper which already has an established hydrodynamic model.
- Final fabrication process to develop the 3d printed microfluidic device with a PCL backing support.
- Characterization of the fabricated channel system. This is done to determine the least printed width and to determine the width of the narrowest hydrophilic channel which could effectively conduct samples.
- Fluid flow analysis.
- Wound parameters- pH and glucose detection. Feasibility of application of the developed μPAD to be demonstrated by dedicating a three-channel system for pH and glucose detection based on colorimetric assays.
- Android app generation and analysis. To develop an application that will read and calibrate the developed color in the test zone based on Hue values to known standards.

The overall idea of the device development as per the above objectives is represented in the figure shown below.

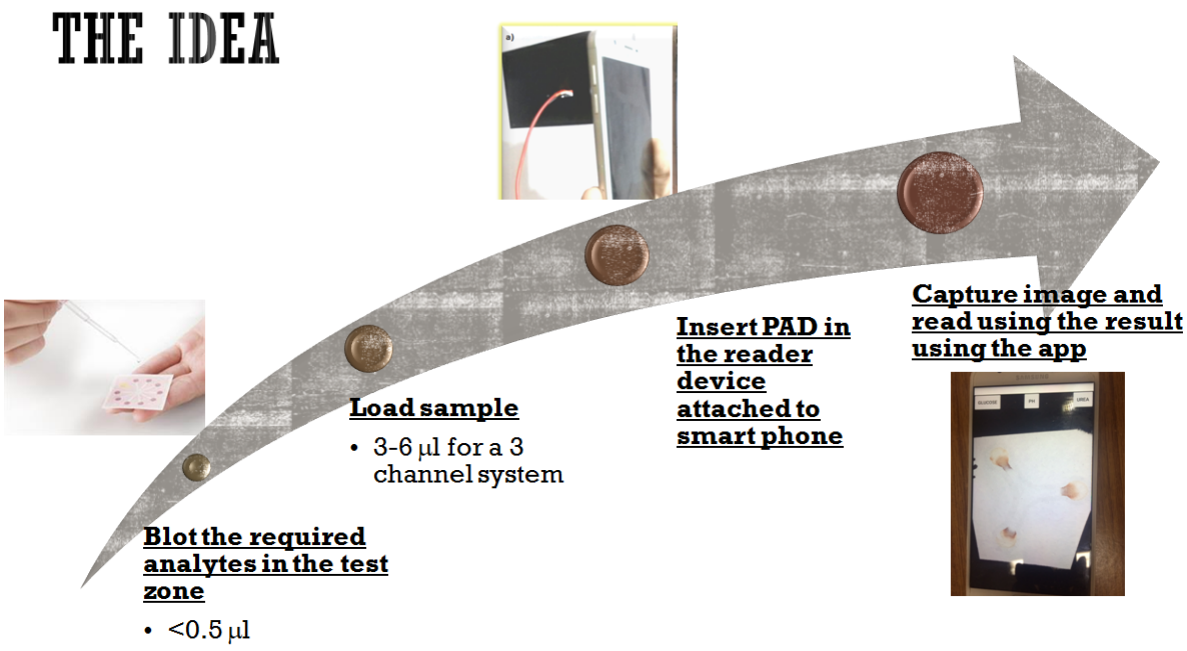

Figure 4: Illustration of the steps involved in the preparation and detection. Once the μPADs are developed, it involves the physical blotting method to input the required analytes (0.5 μl-2 μl) in the test zone. After the time required for drying the blot, 3-6 μl samples may be introduced through the inlet zone. The third step involves the insertion of the PAD, after the sample has reached the test zone, in the reader device which is attached to the smart phone and the fourth step involves capturing the image and reading the result using the developed app.

CHAPTER 2 – MATERIALS AND METHODS

Choice of printing and imaging systems

The syringe based modified form of fused deposition modeling type 3D printer (Makercity, Vandrum Technologies Pvt Ltd) was used throughout the experiments which has a printing area of 45 x 45 cm. The syringe printer head extruded liquid ink filled in a 10mL syringe onto the substrate. The 3D channel systems were designed using 123d design software (Autodesk) and were exported to a stereolithography file format (STL) for 3D printing. Although ink jet printing of microfluidic channels has been extensively explored as a simple and rapid technique, the number of printing cycles and the double-sided printing technique for attaining maximum ink penetration and coverage, needs to be optimized. This is where the use of 3D printing technology is advantageous as it is: -

1) Able to create channels of both simple and complex design
2) Rapid, completely automated with programmable flow speed enabling optimized usage of hydrophobic polymeric ink which further makes the process cost effective.
3) Based on layering approach where layers are printed with better resolution whose penetration depth can be controlled for different substrates based on the thickness and the viscosity of the solution used.
4) Better reproducible and the printed width can be accurately modeled using the hydrodynamic model proposed by Jungchul Kim et al for writing with ink on paper

depending on the substrate, ink and print parameters used for fabrication (140).

For optimization of printing parameters, images of the printed lines were captured using 5x objective of an optical microscope (Leica Microsystems DM400M, Germany) and image analysis was done using the ImageJ software (open source). The fluid flow analysis through the printed channels was done using an android based application (Gonnycam version 2.0.7) for high frequency imaging which captured images at the rate of 5 frames per second.

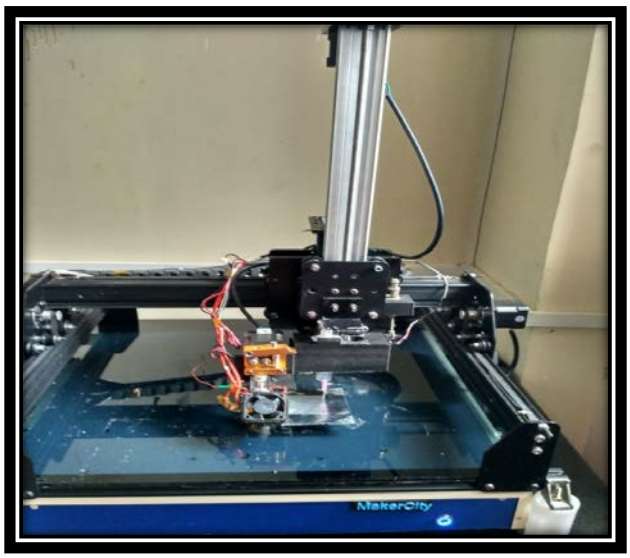

Figure 5: The 3D syringe based printer system (Makercity, Vandrum Technologies Pvt Ltd) used for developing the μPAD

Choice of paper and ink

The key factor in the creation of μPADs is the development of hydrophobic barriers on hydrophilic substrates. Several such porous substrates have been used where the focus is primarily on the improved performance in detection capabilities. In our study, Whatman qualitative filter paper grade 1 was used as the printing substrate which has a pore diameter of 11 microns as it is biocompatible, hydrophilic, homogenous and reproducible (8). Evans et

al conducted a systematic study to analyze the effect of different paper substrates on analytical performance based on colorimetric enzymatic reactions and reported a faster transfer rate and better analytical performance for the grade 1 filter paper (112). For the standardization of the ink concentration, solutions of polycaprolactone (Sigma Aldrich, USA, M_w 70000-90000) in chloroform of different concentrations (w/v%) (3%, 5%, 8%) were assessed for their penetration capabilities. Any overflow of the test liquid (6 µl of simulated thin wound fluid of the following composition: - 0.368g $CaCl_2$, 8.298g NaCl in 100g water) was also noted.

Figure 6: Whatman Filter paper Grade I 150mm diameter which was used for the PAD development process

Standardization of print and printer settings

1) Extruder needle diameter

Using syringe needles of different inner diameters like 0.26 mm (Gauge 26), 0.31mm (Gauge 24), 0.34mm (Gauge 23), single channel systems consisting of circular sample inlet and assay

zones of 3 mm diameter, 10mm hydrophilic channel length and 1.2 mm width were printed (number of layers printed =2). The flow of 3 µL of simulated thin wound fluid in these single channel systems was observed for overflow or leakage. A leakage was reported when the test liquid was wicked across the printed barriers which indicated the absence of hydrophobic barrier deposition. Results obtained were used to standardize the minimum needle diameter required to print the channels which would successfully create a functional hydrophobic barrier in minimum number of layers (2 layers).

2) Layer Height

When extruded, the ink should penetrate the porous Whatman filter paper used as the substrate and the polymer would get deposited between the fiber networks once the solvent evaporates. Hence the process limits the growth of the designed structure to a minimum build up on the surface of the substrate and the minimum layer height possible in Makercity 3D printing systems was chosen.

3) Print Velocity

The print speed was selected as the velocity which provided ample duration between the layers which facilitated complete drying up of a layer before next layer was printed atop, hence preventing any change in width that can arise due to spreading.

Modeling of printing

To identify the parameters that affect the printed width on our substrate while using the syringe based modified fused deposition modeling type 3D printer and to predict an appropriate model to study the effect of using different needle gauge on the printed line width, the process of printing of a single layer was compared to writing with ink on a paper which already has an established hydrodynamic model developed by Jungchul Kim et al. According to the model, width, $w=0.16\eta^2 h +5.55 R$

where $\eta = (\Phi/Ca)^{0.5}$, Υ= surface tension of the ink, h = liquid film thickness, R = radius of nib opening, Φ = surface roughness, Ca, capillary number = $\mu u0/\Upsilon$, μ =viscosity of ink, u0= velocity of pen.

The parameters stated in the above equation which are constant for the presented fabrication technique like surface tension of the ink (Υ), the liquid film thickness (h), the surface roughness (Φ), viscosity of the μ, velocity of pen (u0) (print velocity) were estimated. Viscosity, μ of the ink was measured using Brookfield DV II + (USA) viscometer and the average of those viscosity values obtained for torque above 60 % at rpm ranging from 140-160 was taken using spindle number 61.

Surface tension, Υ of the ink was measured with a dynamic contact angle measurement device (Data physics OCA 15EC, Germany) using pendant drop method. In the pendant drop method, a drop is suspended from a needle in a bulk liquid or gaseous phase. The shape of the drop obtained is determined by opposing forces of gravity and surface tension or interfacial tension. The surface tension seeks to minimize the surface area and get the drop into a spherical shape whereas a gravitational force stretches the drop from this spherical

shape resulting in the typical pear like shape of a drop. Drop shape analysis is performed on the image of the drop for calculating the surface tension (using the software module SCA 22). The analysis of the drop shape is based on the Young-Laplace equation which describes the pressure difference (Laplace pressure) between the areas inside and outside of a curved liquid surface/interface with the principal radii of curvature R_i. (141)

$$\Delta P = (Pint - Pext) = \Upsilon(\frac{1}{R1} + \frac{1}{R2})$$

The height (h) of the liquid film thickness was set as the R_P value (peak roughness) measured by 3D profilometer (TalyMap software) by scanning 2mm. Here when the ink is extruded onto the porous Whatman filter paper used as the substrate, it would get first filled up in the voids or columns on the surface of the filter paper which renders the surface rough and later penetrates the matrix.

Another parameter, surface roughness, Φ was measured as (f-1)/f where f is the ratio of actual area to the projected area of the porous substrate (140). The actual surface area of the substrate was determined using Brunauer–Emmett–Teller analysis in which the specific surface area (m^2/g) is found out using the adsorption of nitrogen gas molecules on the substrate surface.

The velocity of the extruder head, u0 (print speed) is programmable and was chosen as 8mm/sec for the multi-channel design as this velocity provided ample duration between the layers which facilitated drying up of a layer before the next layer was printed. The line width resulting from the use of different needle gauges (23G, 24G and 26G) was predicted using the above model and was compared to the actual width obtained after printing.

Fabrication process

The fabrication of the µPAD was carried out as shown in Figure 4. Using standardized printing parameters, the channels of required design could be printed which would effectively function to distribute the samples introduced, to different assay zones designed in the plane of the paper. The design consists of reservoirs, hydrophilic channels and assay zones. The mechanical strength of the µPAD was further enhanced by introducing a coating of PCL on the rear side which was heat compressed on the rear. This would also reduce the possibilities of contamination. Briefly, 5% (w/v) PCL film is placed on the rear side of µPAD and is sandwiched between aluminum sheets at a pressure of 0.63 psi for 2 minutes while heating at 57-59 °C using a hot plate.

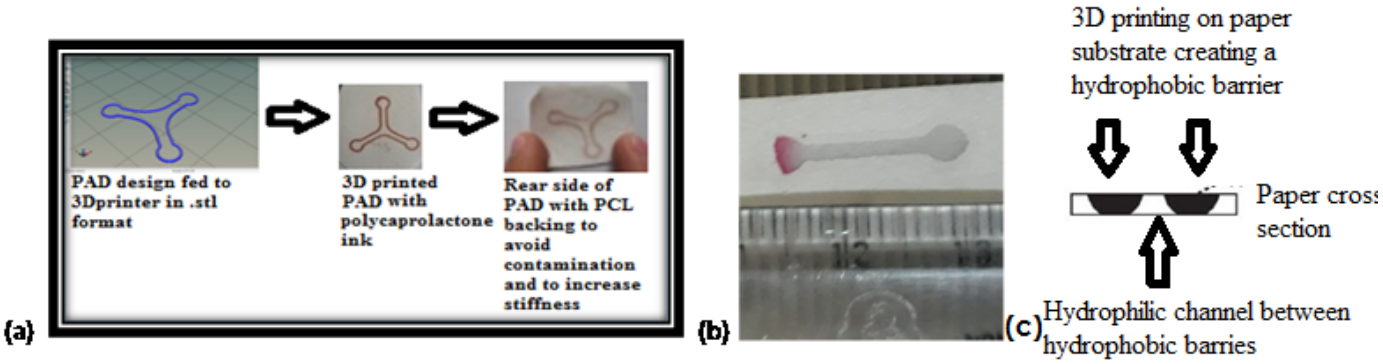

Figure 7: a) Flow chart showing fabrication process of PAD using 3D printed PCL microfluidic channels b) A representative image of a printed single channel PAD tested using simulated thin wound fluid (C) Representation of a 3D printed paper cross section

Characterization of fabricated channel systems

To determine the least printed width which could effectively make a functional hydrophobic barrier, single channel systems of different widths (printed using a 24-gauge needle) were tested for leakage using 3µL of simulated thin wound fluid (no. of layers printed=4). To determine the width of the narrowest hydrophilic channel which could effectively conduct samples, channels of different nominal widths were designed ranging from 1mm to 3mm (using needle gauge 24) were tested for unobstructed sample flow past them. Definitions of a functional hydrophobic barrier and a functional hydrophilic channel were followed as stated by Whiteside's et al. (8). A functional hydrophobic barrier is defined as the one which retained fluid at least for 30 minutes. A hydrophilic channel is defined as the one which conducts fluid from a sample reservoir to assay zone and which is at least 5mm long. The effect of addition of more than 4 layers and the effect of heating (no: of layers printed=4) while introducing the rear side coating of the µPAD on the printed width of the hydrophobic barrier was studied by optical microscopic imaging and analysis performed using ImageJ software.

Fluid Flow analysis in channels

The fluid wet out analysis was conducted on the printed channels (number of layers printed = 4, printed using needle gauge 24) for rabbit blood plasma and simulated thin wound fluid (0.368g $CaCl_2$, 8.298g NaCl in 100g water). For the experiment, 4µL of the samples were added to the single channel systems having the same dimensions as used for leakage tests (single channel systems consisting of circular sample inlet and assay zones of 3mm diameter,

10mm hydrophilic channel length and 1.2mm width). The sample flow was imaged at a rate of 5 frames per second using an android based application for high frequency imaging (GonnyCam). The graph of distance covered starting from the neck of the straight channel, L against the square root of time taken to cover the distance, √t was plotted cumulatively.

Preliminary studies for two analyte detections

The developed µPAD was coupled to colorimetric mode of detection for the simultaneous quantification of glucose and pH of wound fluid by developing an android based application which can be used to capture the image and interpret the results. Three channeled microfluidic devices were used for these applications.

Glucose estimation

The colorimetric detection of glucose is achieved by an enzymatic reaction where a mixture of glucose oxidase and horseradish peroxidase in the presence of starch-potassium iodide solution reacts with glucose to give a blue black colored starch tri iodide complex. In this reaction glucose is oxidized to gluconic acid and hydrogen peroxide, which is reduced to water while potassium iodide (KI) is reduced to Iodine. Iodine and remaining iodide form triiodide ions which gets entrapped in starch to give the blue black colored complex. As the concentration of glucose in the sample increases the colorimetric intensity of blue black also increases. Glucose estimation studies were carried out in a three-channel system using 6µL of the glucose standard solutions of different concentrations ranging from 0.5mM to 20 mM

(0.5,1.5,3,5,10,20).

Preparation of assay zone

Initially, a solution of trehalose – starch-KI solution was prepared in PBS (trehalose-1.13g, KI-0.996g, starch-100mg in 10ml of PBS) and 2µL of the solution was blotted to the assay zone sequentially and dried. Equal volume of glucose oxidase (250U/ml) and horseradish peroxidase (50U/ml) were mixed and 2 µL of the mixture was sequentially blotted on to the assay zone. After drying the assay zone perfectly, sample solutions (6 µL) were introduced and images were captured after making sure that the sample solution is completely wicked to the assay zone.

pH estimation

For pH estimation studies the pH indicator used was anthocyanin extracted from red cabbage *Brassica oleraceae* which is a cost effective and biocompatible choice. It can produce notable color change in wide range from acidic to alkaline.

Anthocyanin extraction - Fifteen grams red cabbage was finely minced in pestle and mortar by adding 10 ml of 1 % HCl–methanol. The mixture was transferred in a centrifuge tube and kept overnight in refrigerator for extraction of anthocyanins. Next day, 5 ml of chloroform and 4 ml of distilled water were added to the mixture. It was then centrifuged for 30 min at 3000 rpm. Supernatant thus obtained was transferred to an amber colored bottle and kept in refrigerator for future use (142).

For the calibration single channel systems of well diameter 3mm and channel width 1.2 mm were used. Buffers used for the calibration are shown in table 1.

Measured pH	Buffer system
2.36	Citric acid buffer
7.25	Phosphate buffer
8.93	Potassium chloride-sodium hydroxide buffer
11.06	Potassium chloride-sodium hydroxide buffer
4 and 7	Ph meter calibrating solution

Table 1: Table depicting the measured pH and the buffer systems used in the study

The preparation of the different buffer systems is detailed below

1) **Citrate buffer (pH=2.36)**

Reagents required: -

- Citric acid: - Dissolve 2.101g of citric acid in 100 ml distilled water.
- Sodium citrate solution 0.1M: Dissolved 2.941g of sodium citrate in 100ml distilled water

Procedure –Take 46.5 ml citric acid with 3.5 ml of sodium citrate solution and make up to 100ml with distilled water. It corresponds to 0.1M citrate buffer.

2) **Phosphate Buffer (pH=7.25)**

Reagents required: -

- Monobasic: - Dissolve 2.78g of sodium dihydrogen phosphate in 100 ml of distilled

water

.• Dibasic sodium phosphate(0.2M): - Dissolve 5.3g of disodium hydrogen phosphate or 7.17g Sodium hydrogen phosphate in 100 ml distilled water.

Procedure: - 39ml of dihydrogen sodium phosphate is mixed with 61 ml of disodium hydrogen phosphate. This is made up to 200 ml with distilled water. This gives phosphate buffer of 0.2M.

3) **Potassium Chloride-Sodium hydroxide (pH=8.93)**

Stock solutions: -

- Solution A: 0.2M solution of KCl (14.9g KCL in 1-liter water)
- Solution B:-0.2 M solution of NaOH (8g NaOH in 1 litre water)

Procedure: - Mix 25ml of A and 6 ml of B and dilute to 100 ml with distilled water and made to pH 8.93.

Preparation of the assay zone

The assay zone was sequentially blotted with 2µl of anthocyanin indicator and dried. 4 µL of different buffer solutions were introduced after drying the assay zone.

Red Cabbage Color changes with pH

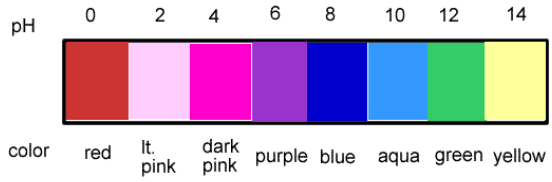

Figure 8: Illustration of the pH based color change when using anthocyanin as the pH indicator.

Imaging system

The images were captured using smartphone camera by inserting the PADs which has developed a color change in its assay zone, into a slot on the reader device connected to the smart phone. The reader device was utilized to provide uniform lighting and focusing for capturing the images. The reader device was illuminated inside by using 2 LEDs which were powered by the smartphone using microUSB. The smart phone used had a camera resolution of 13MP.

Figure 9: Black reader device which can be fixed onto the smartphone device. The device houses a slit on the top surface to introduce the μPAD and 2 LED lights illuminate the black reader box from either side. The LED lights are powered by the phone power using microUSB OTG connection.

The images were cropped to the colored areas i.e. blue-black for glucose estimation and respective colors for pH estimation and average HSV coordinates [Hue, Saturation, Value] of the image where calculated and calibrated.

Algorithm of developed android based application for detecting the colorimetric reaction

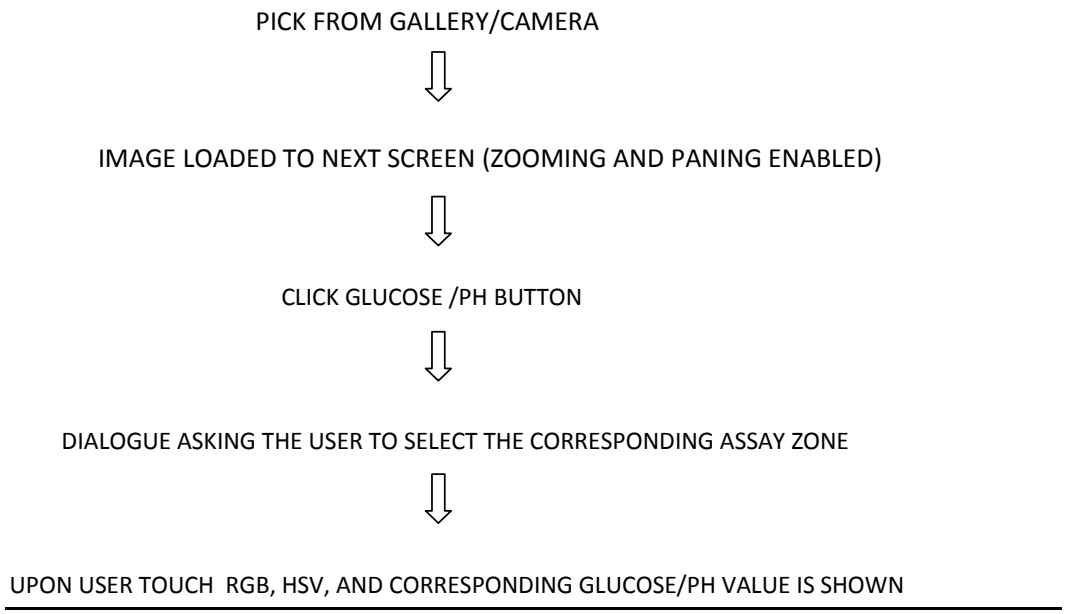

Figure 10: Algorithm of developed android based application for detecting the colorimetric reaction

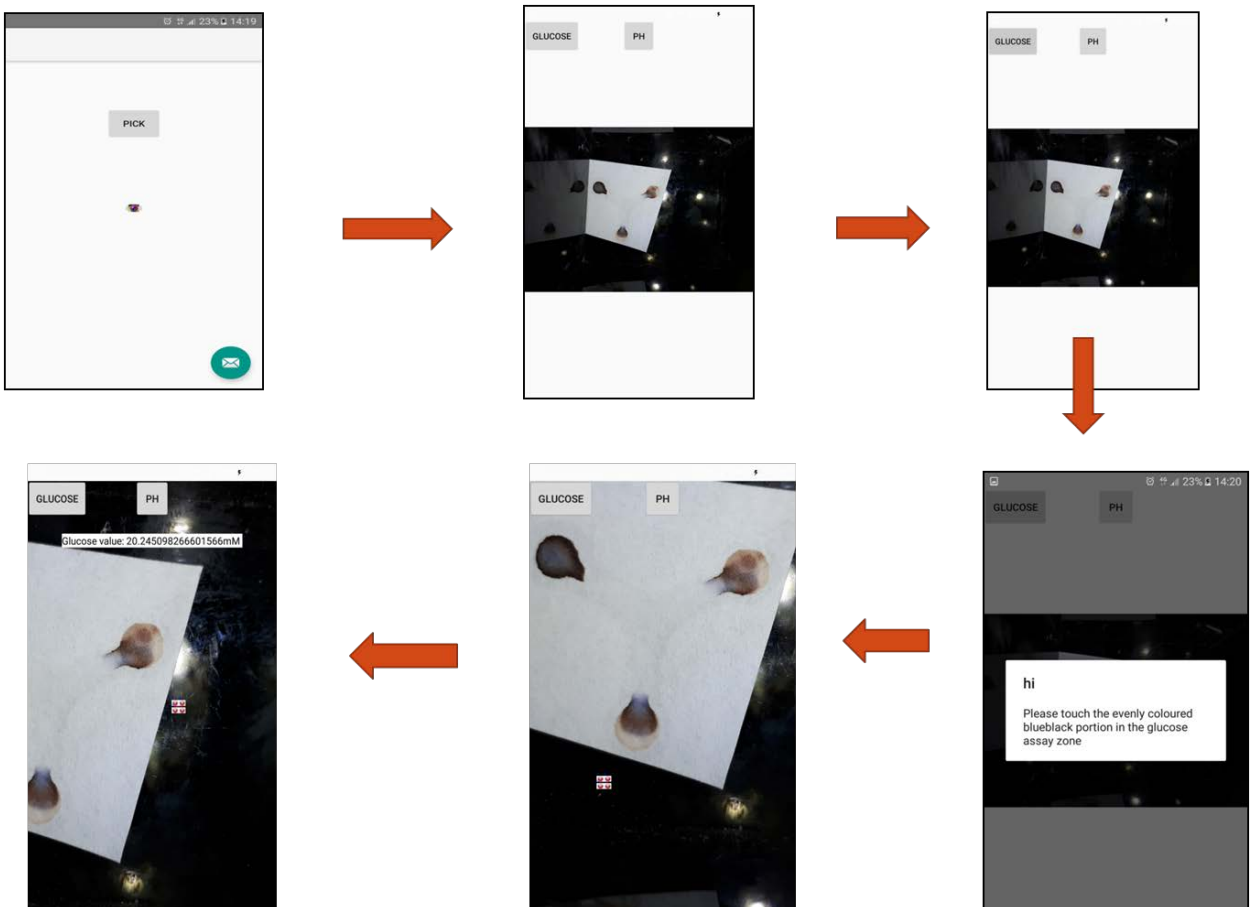

Figure11: Screen shots depicting control flow of the developed android application

CHAPTER 3 – RESULTS AND DISCUSSION

Choice of ink and print settings

In this study solutions of polycaprolactone in chloroform of different concentrations (w/v%) (3 %, 5%, 8 %) were prepared and assessed for their viscosity and penetration capabilities. The viscosity values are reported in table 2. The channels printed using 8% concentrations of PCL in chloroform showed a highly viscous behavior with a viscosity of 123.7±2.75 cP and hence could not penetrate sufficiently to form a hydrophobic barrier which resulted in the overflow of the test liquid through barrier less portions. The channels printed with 3% (w/v%) PCL in chloroform (viscosity- 19.4±0.05 cP) showed positive results as the number of layers were increased to 10 but failed when the number of layers were minimized to 2 as the polymer deposition was insufficient and there was incomplete hydrophobic barrier which resulted in the leakage through the voids of hydrophobic barrier. The polymer deposition was however comparatively less at 10 layers and the printed width exhibited a greater deviation from nominal width due to the high volatility of the ink and hence it affected the reproducibility of the channel width. The channels printed with 5 w/v% PCL in chloroform with a viscosity of 35.4 ± 1.23 cP could successfully retain the fluid within the barrier limits and prevented its overflow by forming a functional hydrophobic barrier at the minimum print of two layers with consistency in printed width. Hence the concentration of the ink chosen for preparing the channels was 5% (w/v %) solution of PCL in chloroform.

Concentration Of PCL (w/v%)	RPM	Spindle Number	%Torque range	Temperature range (°C)	Viscosity (cP)
3	200	61	60-70	25-26	19.4±0.05
5	120	61	60-70	25-26	35.4±1.23
8	150	62	60-70	25-26	123.7±2.75

Table 2: The viscosity of the different concentrations of PCL (w/v %) in chloroform

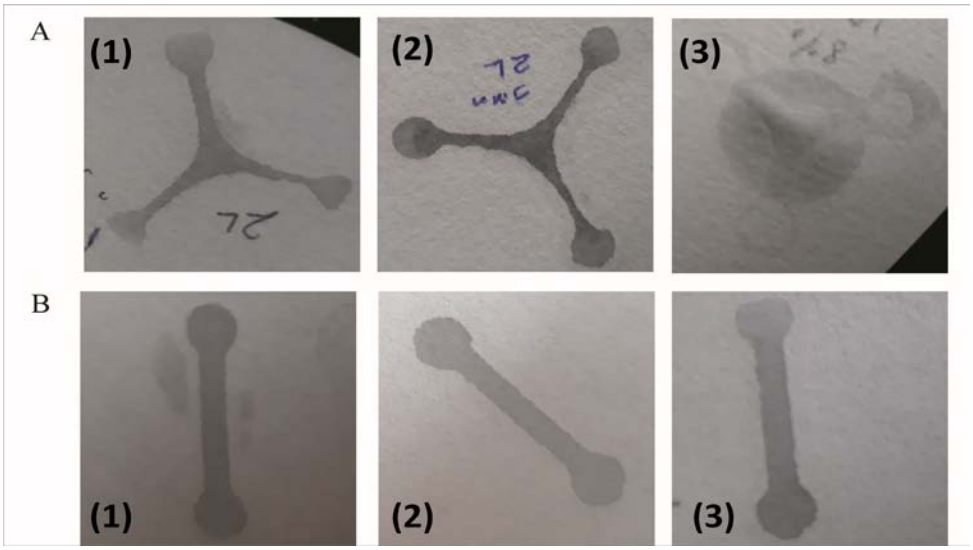

Figure 12: A) Standardization of PCL ink concentration by leak test, (1) 3%, (2) 5% and (3) 8%; B) Leakage test when using different needle diameters (1) 26 G, (2)24 G, (3) 23 G

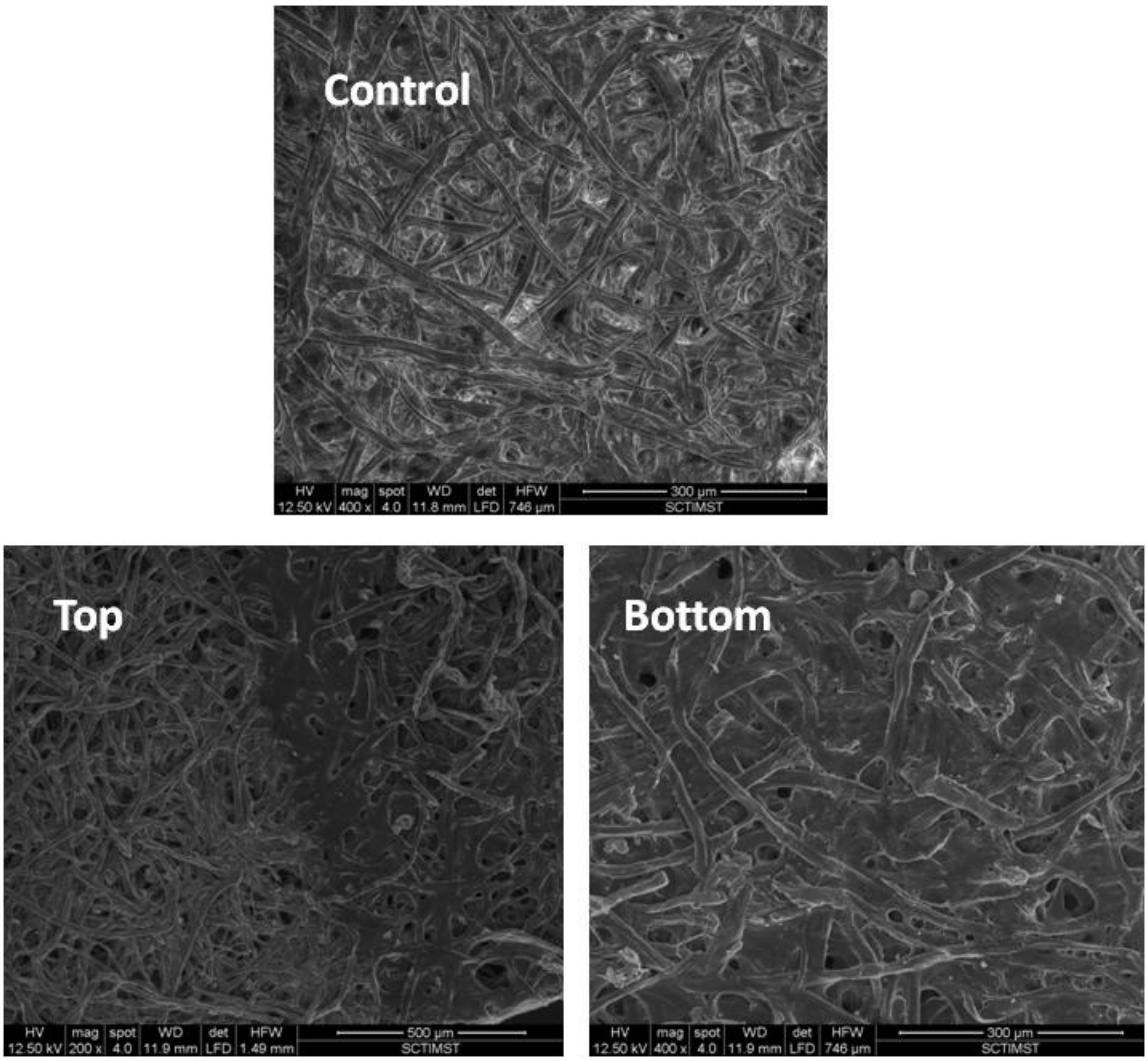

Figure 13: SEM images showing the control, top and bottom surface of a fabricated PAD

The print parameters were also assessed, and the results are as shown in the Table 2. It was observed that the creation of an effective hydrophobic barrier required at least a minimum buildup of two layers. The use of needles with gauge 24 and 23 created channels with good hydrophobic barrier penetration (in a minimum print of two layers) than when printed with a smaller needle diameter where seepage of test fluid through the barrier was observed (for two layers) shown in Fig 8(b). The layer height set at 65 microns ensures that dripping of the

ink from the extruder is avoided until the termination of printing. The printer speed was standardized as 8mm/sec according to the design used to ensure the complete drying of the layers prior to the printing of the next layer atop.

Sl No:	Parameter	Value
1	Speed: Perimeters, Small perimeters, External perimeters, First layer	8mm/sec
2	Extruder needle diameter	0.31 mm
3	Layer height	65 microns
4	Layer range	2-4

Table 3: The print parameters that has been standardized for the printing process

Modeling of printing

Here we have assumed that the process of ink extrusion from the syringe module of fused deposition type 3D printer on a porous substrate like paper to be like the mechanism by which ink is extruded on paper while writing with a basic pen (which has a long narrow tube that serves as a reservoir of liquid) whose hydrodynamical model has been established by Jungchul Kim et al. (140). According to the hydrodynamical model proposed by Jungchul Kim et al., while writing with ink on paper the parameters on which the width of the trail left as the nib moves forward depends on the following parameters; i) Properties of the ink used like viscosity (μ) and surface tension (ϒ) ii) properties of the substrate like surface roughness (Φ) iii) Velocity of the nib (u_0) iv) the height of the liquid film thickness and v) radius of the nib opening (R). To compare the established process of fabrication with this model, all the other parameters except R is maintained constant and the width of the line was predicted using different R values (needle diameters) as in this case and compared to the experimental results. A graph was then

plotted with the needle diameter (mm) against the width (mm) as shown in the graph (both experimental and theoretical). It is seen that the model slightly overpredicts the experimental value which was also observed by Jungchul Kim et al. which may be due to the high volatility and non-Newtonian behavior of the ink used. Hence the results depict that the model can be effectively used to explain the printed width in the above fabrication process.

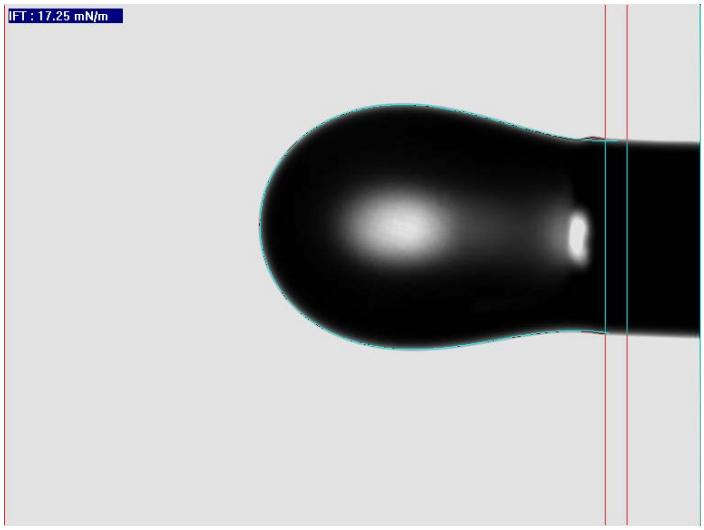

Figure 14: Representative image of the drop profile for measurement of surface tension using the pendant drop method in contact angle testing.

Calculation of Φ from BET data

Φ=f-1/f

f= (Actual area from BET analysis/g) /(projeced area/g)

= (0.83/g) / (0.0845/g) =9.8225

Hence Φ=0.898

(a)

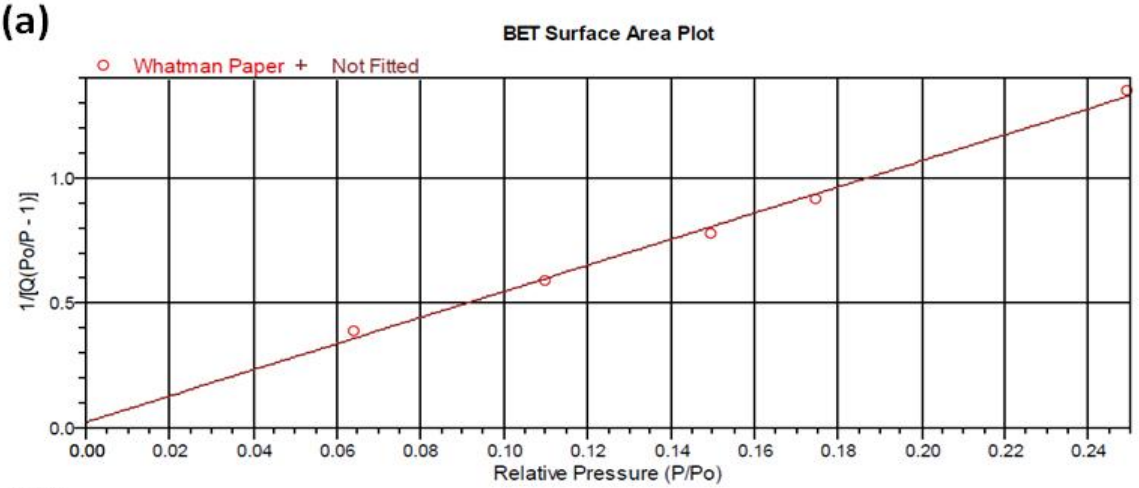

(b)

Figure 15: (a) Calculation of the Surface roughness (ϕ) from BET analysis, (b) BET surface area plot of Relative pressure (P/Po) against 1/[Q(P0/P-1]

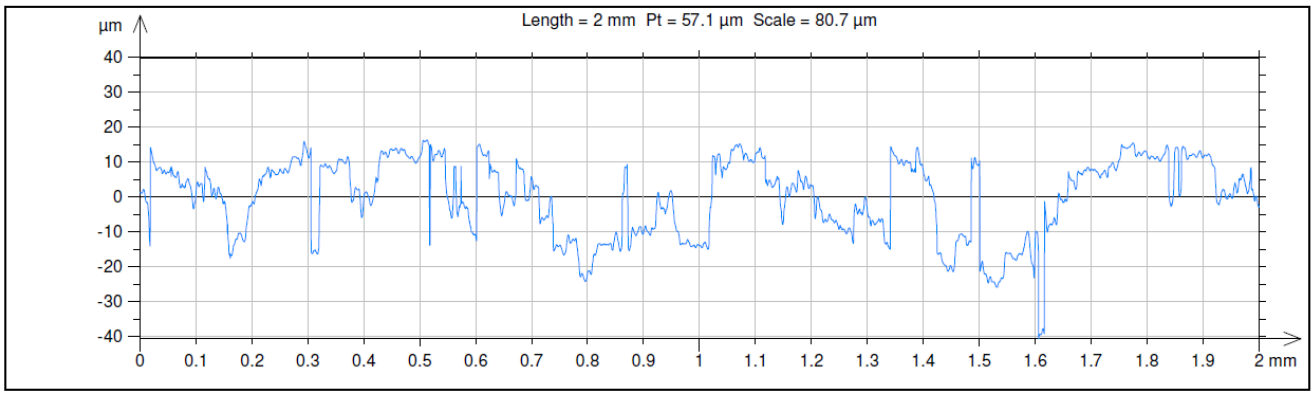

Figure 16: Profilometric plot for calculating the liquid film height (h)

Sl No:	Surface Tension, ϒ (N/m)	Viscosity (Pa. S)	Velocity, u_0 (m/s)	Height of liquid film, h (m)	Roughness factor, Φ	Radius of the needle opening, R(m)	Theoretical width (mm)	Experimental width (mm)
1	0.017±0.00025	0.036±.001	0.008	$5.4x10^{-6}$	0.898	$0.13x10^{-3}$	1.019	0.79±0.057
2	0.017±0.00025	0.036±.001	0.008	$5.4x10^{-6}$	0.898	$0.155x10^{-3}$	1.158	0.866±0.12
3	0.017±0.00025	0.036±.001	0.008	$5.4x10^{-6}$	0.898	$0.17x10^{-3}$	1.24	1.003±0.062

Table 4: The parametric results obtained for each of the parameters used for simulating the hydrodynamical model for comparison of the print width with the experimental printed width (mm). The hydrodynamical modeled width is calculated as per the equation, width, $w=0.16\eta^2h+5.55$ R where $\eta = (\Phi/Ca)^{0.5}$, ϒ= surface tension of the ink, h = liquid film thickness, R = radius of nib opening, Φ = surface roughness, Ca, capillary number = μu0/ϒ, μ =viscosity of ink, u0= velocity of pen.

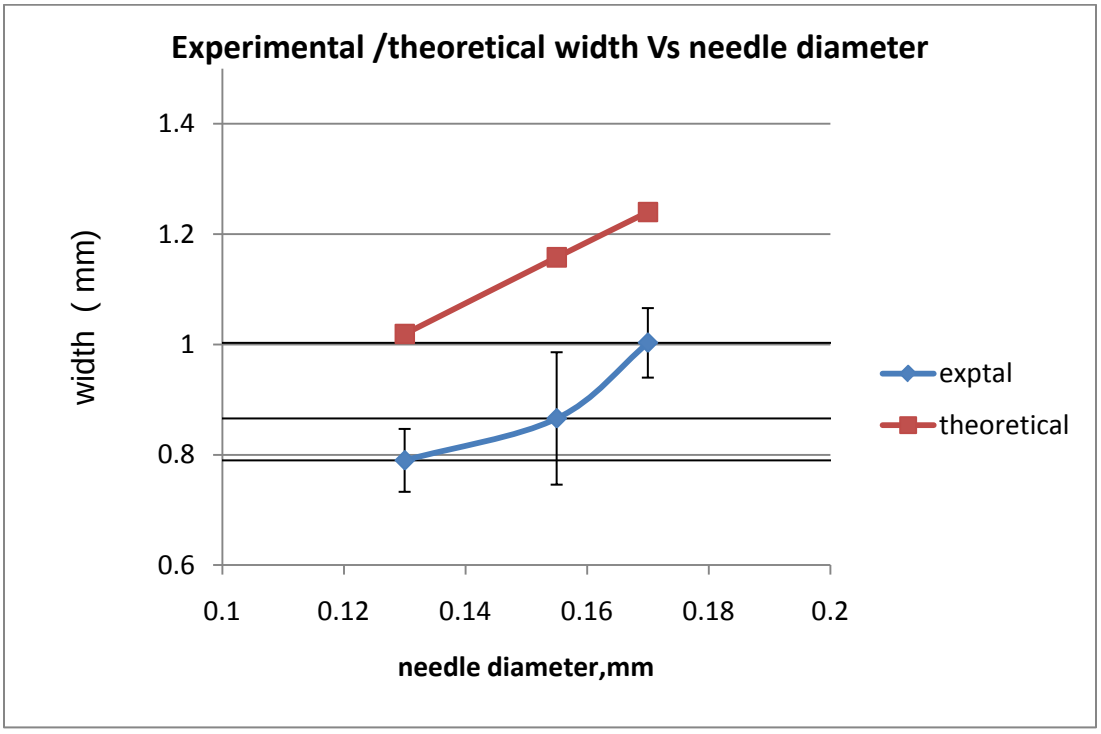

Figure 17: Plot of needle diameter, mm Vs width (mm). The linearity and correlation of the experimental width with the needle diameter is evident from this graph.

Characterization of printing

The results from the leakage test shows that a functional hydrophobic barrier was obtained at a minimum printed width of 0.866 ± 0.12mm. Also, the minimum conducting width of the hydrophilic channel was found to be 460.7 ± 20 µm. Whiteside's et al. reported a minimum functional hydrophilic channel width of 561 ± 45µm by wax printing whereas Yong He et al reported a minimum functional channel width of 118 ± 17µm for 3D printed PDMS PADs. In the case of other fabrication methods like inkjet etching and laser cutting a much finer resolution was achieved due to improved precision. The analysis of the effect of layer addition on the printed width (above 4 layers) suggest that the layers beneath already rendered the surface hydrophobic which confines the spreading of the ink further and hence mostly maintains the printed width. The analysis of the effect of heating on the printed width suggest that there is no major influence since the temperature used during the fabrication of the backing support of PCL (57-59 °C) on the rear would just render the polymer sticky to adhere to the rear without melting. If melting occurred, it may result in further widening of the printed width.

Number of layers added	Printed width (microns)
4	1340.04 ± 247.26
5	1348.4 ± 85.724
6	1350.2 ± 118.75
7	1348.2 ± 112.5
8	1348.1 ± 110.5
9	1434.7 ± 141.3
10	1343.5 ± 100.9

Table 5: Table depicting the width of the printed lines on deposition on deposition of layers (4 to 10)

Width of line before heating(µm)	Width of line after heating(µm)
982.2 ± 142.75	1065.3 ± 40.06
1328.4 ± 115.72	1337.8 ± 66.9
1475.79 ± 189.34	1496.47 ± 115.28
1549.72 ± 72.77	1555.88 ± 96.06

Table 6: Table depicting the width of the printed line before and after heating while applying the backing support of PCL.

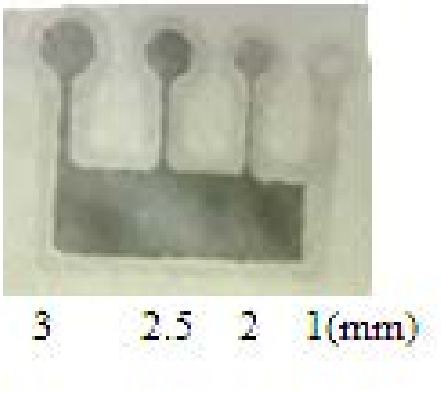

Figure 18: Design used for finding minimum hydrophilic channel width. Channel widths (1mm, 2mm, 2.5mm and 3mm) were explored in this study.

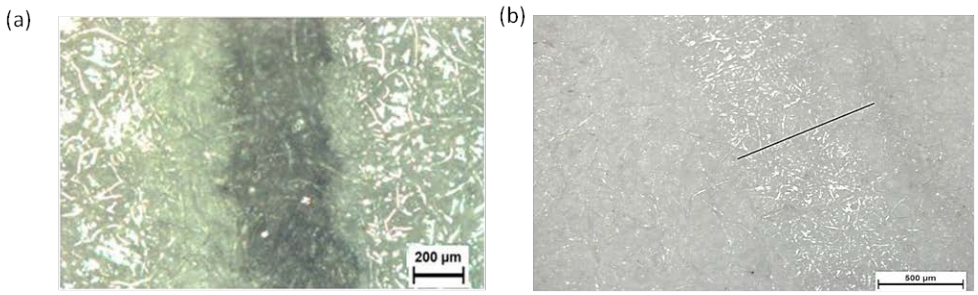

Figure 19: A representative image of (a)minimum hydrophilic channel and (b) minimum hydrophobic barrier width imaged under 5X objective of an optical microscope system. The image was analyzed using ImageJ software.

Fluid flow analysis

The graph of "L" Vs "sq. rt of t" shows a linear trend which is in conformity with the famous Washburn model for fluid flow through porous media (85). Washburn model suggests that $L=(\gamma Dt/4\eta)^{1/2}$ where L is the distance that a liquid of viscosity η and surface tension γ penetrates a porous material with an average pore diameter D in time t. From the data, the time taken by both rabbit blood plasma and simulated thin wound fluid to traverse the channel and reach the assay zone as designed is around 195 sec. This data gives an insight into the optimization of the channel design based for future applications.

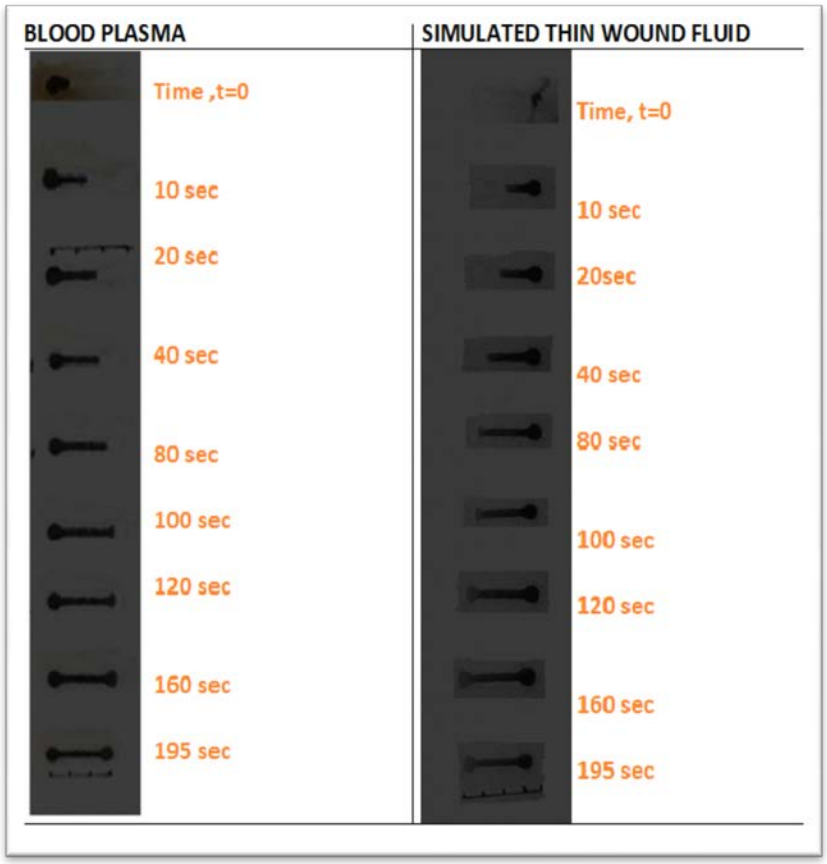

Figure 20: Figure showing the time taken by both rabbit blood plasma and simulated thin wound fluid to traverse the channel and reach the assay zone. Both the fluids were able to reach the test zone in 195 sec.

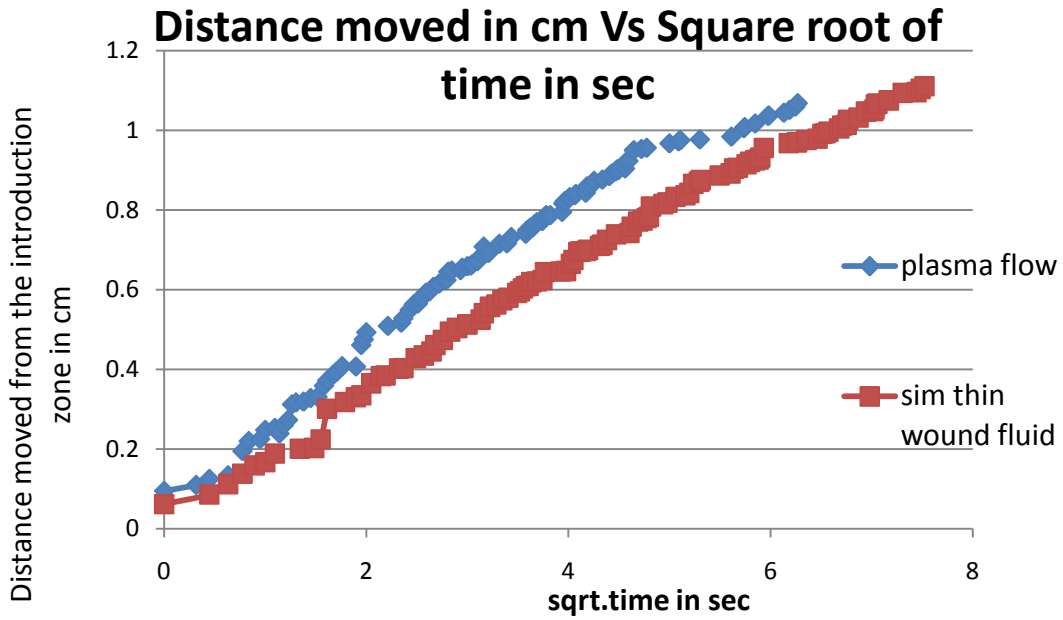

Figure 21 : Graph depicting the distance moved in cm Vs the square root of time in sec.

Preliminary studies for two analyte detection

Glucose estimation

The images captured using the imaging system were cropped into a uniform region of blue black color to determine the average hue, saturation and value coordinates of the area. The images obtained for increasing concentration of glucose showed to have decreasing average value coordinates. The graph of concentration of glucose versus corresponding value coordinates showed a linear curve with a negative slope of -1.51.

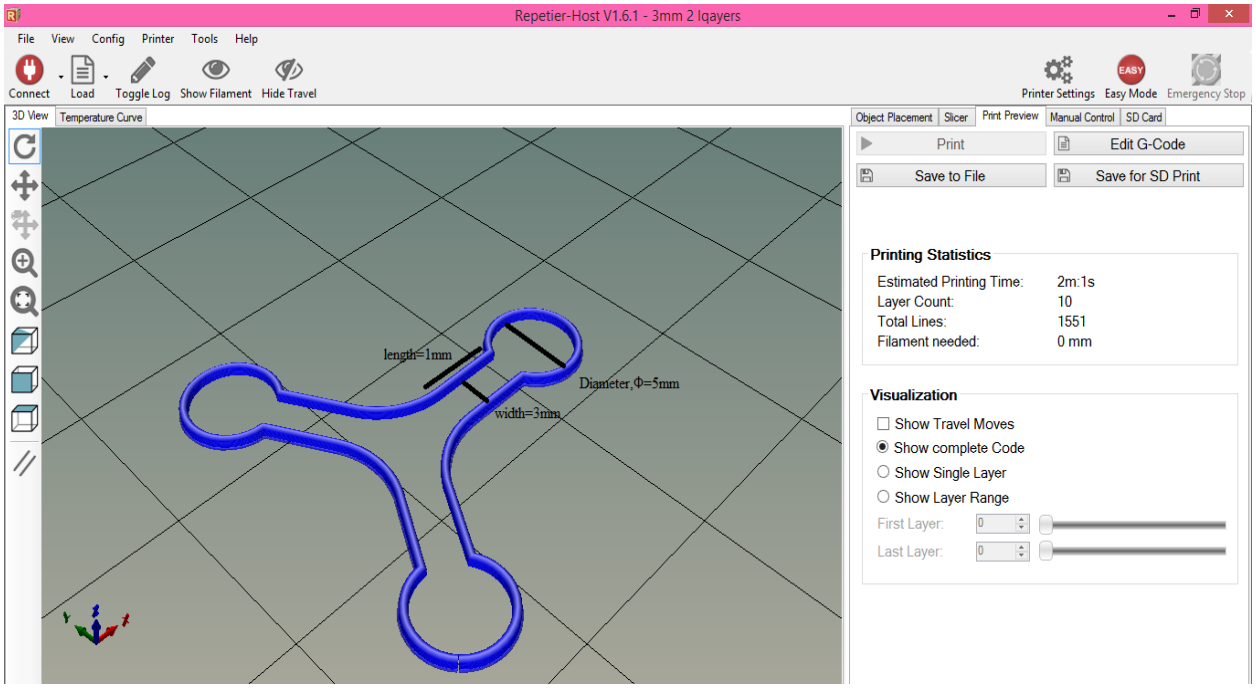

Figure 22: Three channel system with three assay zones used for glucose estimation where sample is introduced at center. Solid drawing was taken with an infill of 0% where the perimeters were only considered. The length of the channel between the inlet and assay zone was 1cm and the diameter of the test zone being around 5mm.

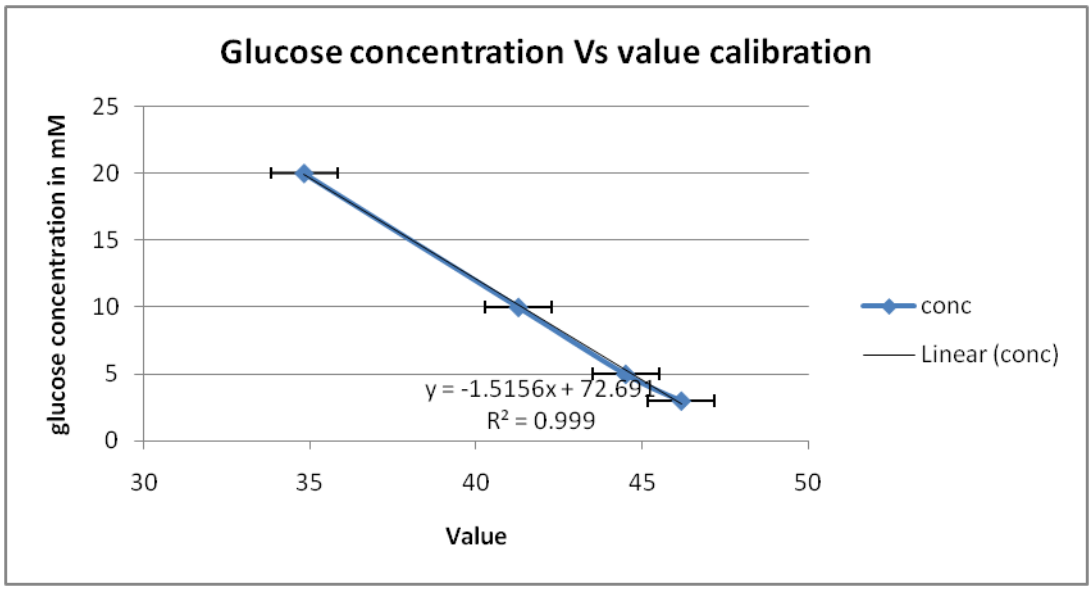

Figure 23: Graph showing the concentration of standard Glucose solutions in mM against the value coordinate (LoD = 3 mM , sensitivity = 0.66)

Val coordinate	Concentration of glucose in mM/L
46.175±0.417	3
44.5±1.77	5
41.275.±3.34	10
34.83.±1.11	20

Table 7: The value coordinates corresponding to the concentration of glucose in mM/L

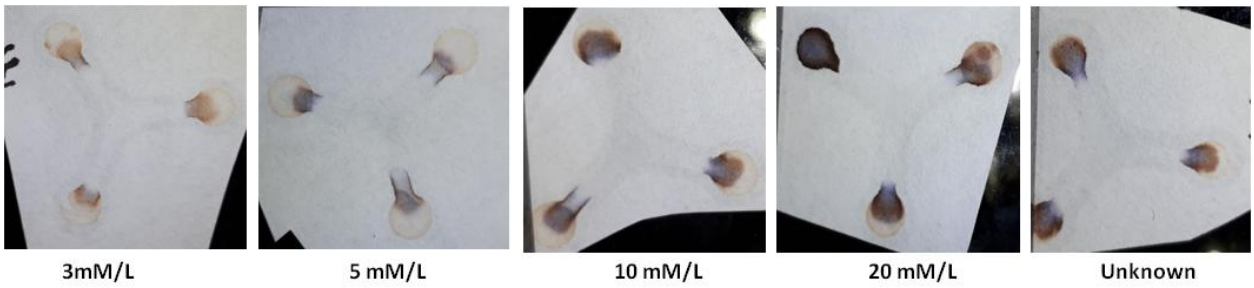

Figure 24: The blotted results of the different standard glucose solutions used to prepare the calibration curve. An unknown sample was also attempted to find the accuracy of the calibration done using 7mM/L Glucose solution.

Calculation of concentration from the calibration curve

The image of the unknown was captured by introducing 7Mm of glucose standard solution to a µPAD with prepared assay zones for glucose estimation. After cropping the image, average value coordinate was calculated as earlier which was equal to 43.815. From the calibration curve y=-1.5156x +72.691, calculated concentration of glucose is 6.28Mm which shows a deviation of 0.715 from the actual concentration.

pH estimation

The images were captured after introducing different buffer systems corresponding to different pH. The anthocyanin indicator gave the color changes which corresponded to different hue values. The images were cropped, and uniform color distribution and average hue values were calculated as earlier.

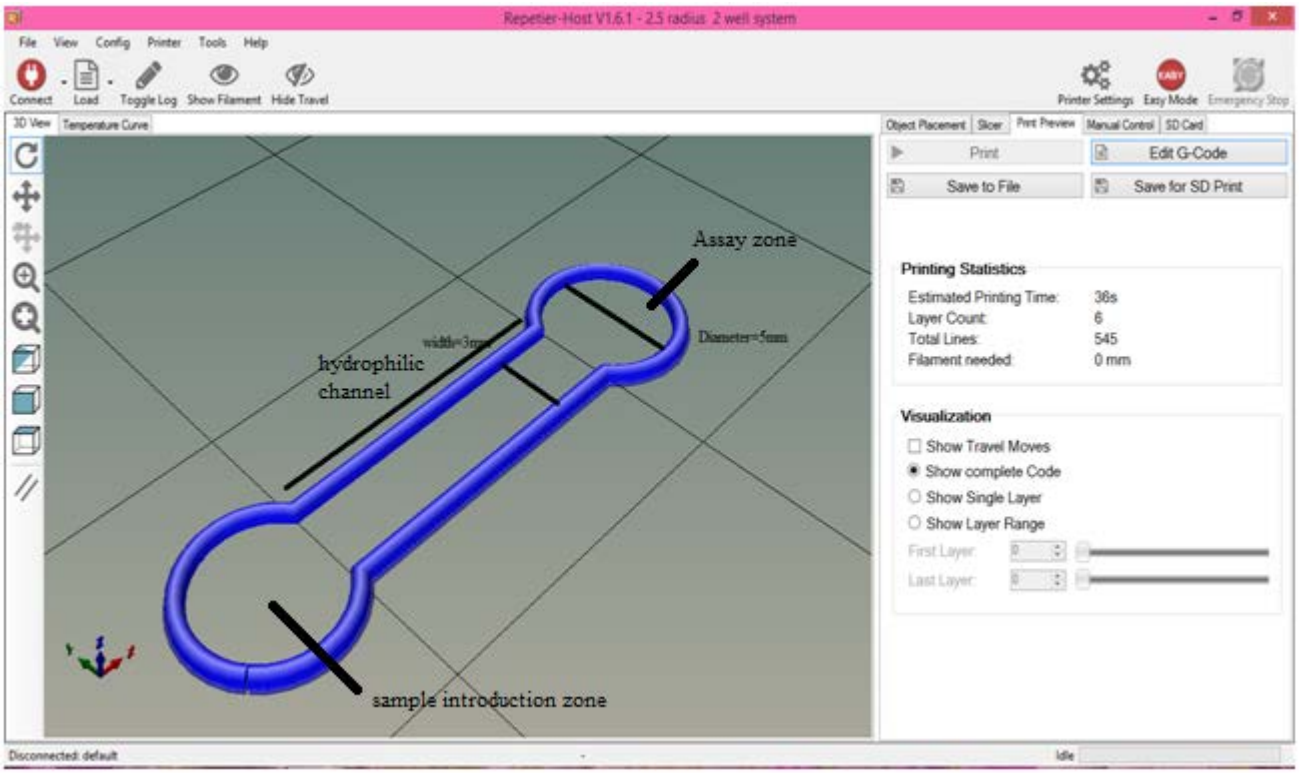

Figure 25: Two channel system used for pH estimation. Solid drawing was used with an infill of 0% where the perimeters were only considered. The length of the channel between the inlet and assay zone was 1cm and the diameter of the test zone being around 5mm.

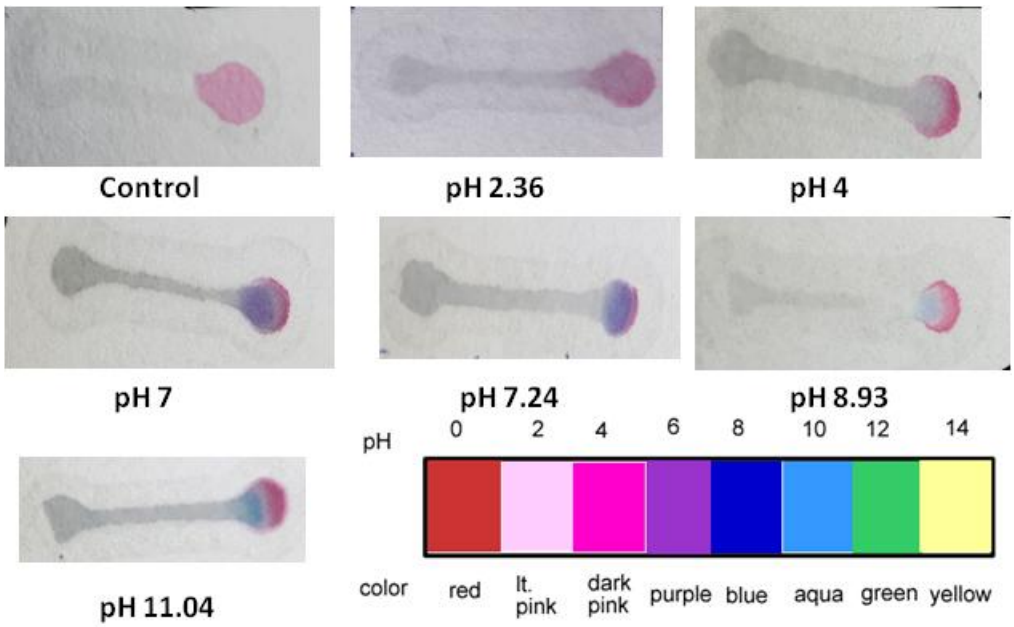

Figure 26: The initial blotted results (before full wet out) of the different standard pH solutions used to prepare the calibration curve. The color was in accordance with the pH color scale in the entry area of the assay zone with a pink corona which indicates the color of the control.

Hue	**pH**
0.1±0.01	2.36
0.08±0.01	4
0.712±0.006	7
0.665±0.005	7.25
0.608±0.02	8.93
0.615±0.049	11.04

Table 8: The value coordinates corresponding to the pH.

Results show that this method of detecting wound fluid glucose level and pH shows good sensitivity though it can be improved further. Other aspects of this sensor like improvement of LoD, sensitivity and inclusion of more analytes can be further studied on.

SUMMARY AND CONCLUSION

The potential of 3D printing in the arena of fabrication of microfluidic devices has already been explored, and proves to be a powerful technique with several advantages over the existing methods like soft lithography. But the advent of 3D printing to field of paper based microfluidic devices fabrication which further enhances the efficacy of point of care diagnostics making them cost effective is yet to be marked. This study provides an insight into the potential of 3D printing to revolutionize this field by making the fabrication of paper based microfluidic devices extremely rapid (one step) and highly cost effective and programmable. The results also depict that this approach is as effective as the other existing methods of fabrication in terms of accuracy and flexibility. The presented study characterizes the printing process and modeling gives an insight to the parameters that could influence printing which makes the process more reproducible and programmable. The fluid flow pattern in the device is also demonstrated which is important from the point of view of device designing. The application of the device as a multianalyte sensor system detecting pH and Glucose based on a colorimetric mode of detection of simulated wound fluid is an example of the multiple utilities where paper based microfluidic devices can be employed. The presented work hereby provides a vivid analysis of the prospective of 3D printing in the fabrication of two-dimensional paper based microfluidic devices. The development of this novel methodology to design and develop a µPAD to evaluate or monitor wounds fluids for parameters that would help clinicians to diagnose wound healing will contribute to developing the technology of diagnostic therapies for wound analysis accessible to patients in low resource settings in a very cost-effective manner.

FUTURE PERSPECTIVES

The present study has considered the development and characterization of a 3D printed microfluidic paper based device and its application for detection of two wound fluid parameters- pH and Glucose. More future studies are warranted in this area of study which includes

- Development of four or more channel systems for multi analyte detection.
- To study more wound healing parameters like urea, C reactive proteins, total protein content, nitric oxide, reactive oxygen species etc.
- To develop the app system to read more analytes and to calibrate the software to the standards used and to calibrate the system based on the camera resolution.
- To design and develop a cost-effective paper board based reader device which can fit on any smart phone for easy readability.
- To validate the production of the PAD for efficient scale up process.

REFERENCES

1) Izmailov NA, Shraiber MS. A drop-chromatographic method of analysis and its applications to pharmacy. Farmatsiya. 1938;3:1-7.

2) Shostenkot YV, Georgievskii VP, Levin MG. History of the discovery of thinlayer chromatography. Journal of Analytical Chemistry. 2000 Sep 1;55(9):904-5.

3) Whitesides GM. The origins and the future of microfluidics. Nature. 2006 Jul 27;442(7101):368-73.

4) https://www.elveflow.com/microfluidic-tutorials

5) Lisowski P, Zarzycki PK. Microfluidic paper-based analytical devices (μPADs) and micro total analysis systems (μTAS): development, applications and future trends. Chromatographia. 2013 Oct 1;76(19-20):1201-14.

6) Sia SK, Linder V, Parviz BA, Siegel A, Whitesides GM. An Integrated Approach to a Portable and Low-Cost Immunoassay for Resource-Poor Settings. Angewandte Chemie International Edition. 2004 Jan 16;43(4):498-502.

7) Sia SK, Whitesides GM. Microfluidic devices fabricated in poly (dimethylsiloxane) for biological studies. Electrophoresis. 2003 Nov 1;24(21):3563-76.

8) Martinez AW, Phillips ST, Butte MJ, Whitesides GM. Patterned paper as a platform for inexpensive, low-volume, portable bioassays. Angewandte Chemie International Edition. 2007 Feb 12;46(8):1318-20.

9) Müller RH, Clegg DL. Automatic paper chromatography. Analytical Chemistry. 1949 Sep 1;21(9):1123-5.

10) Li X, Ballerini DR, Shen W. A perspective on paper-based microfluidics: current status and future trends. Biomicrofluidics. 2012 Mar;6(1):011301.

11) Petryayeva E, Algar WR. Toward point-of-care diagnostics with consumer electronic devices: the expanding role of nanoparticles. Rsc Advances. 2015;5(28):22256-82.

12) Sun J, Xianyu Y, Jiang X. Point-of-care biochemical assays using gold nanoparticle-implemented microfluidics. Chemical Society Reviews. 2014;43(17):6239-53.

13) Goryacheva IY, Lenain P, De Saeger S. Nanosized labels for rapid immunotests. TrAC Trends in Analytical Chemistry. 2013 May 31;46:30-43.

14) Rosenstein RW, Bloomster TG, inventors; Becton Dickinson, assignee. Solid phase assay employing capillary flow. United States patent US 4,855,240. 1989 Aug 8.

15) Gordon J, McMahon ME, Ching S, inventors; Abbott Laboratories, assignee. Chromatographic test strip for determining ligands or receptors. United States patent US 4,960,691. 1990 Oct 2.

16) Haeberle S, Zengerle R. Microfluidic platforms for lab-on-a-chip applications. Lab on a Chip. 2007;7(9):1094-110.

17) Yetisen AK, Akram MS, Lowe CR. based microfluidic point-of-care diagnostic devices. Lab on a Chip. 2013;13(12):2210-51.

18) Posthuma-Trumpie GA, Korf J, van Amerongen A. Lateral flow (immuno) assay: its strengths, weaknesses, opportunities and threats. A literature survey. Analytical and bioanalytical chemistry. 2009 Jan 1;393(2):569-82.

19) Cate DM, Adkins JA, Mettakoonpitak J, Henry CS. Recent developments in paper-based microfluidic devices. Analytical chemistry. 2014 Nov 21;87(1):19-41.

20) Yetisen AK, Akram MS, Lowe CR. based microfluidic point-of-care diagnostic devices. Lab on a Chip. 2013;13(12):2210-51.

21) Liana DD, Raguse B, Gooding JJ, Chow E. Recent advances in paper-based sensors. Sensors. 2012 Aug 24;12(9):11505-26.

22) Ispas CR, Crivat G, Andreescu S. recent developments in enzyme-based biosensors for biomedical analysis. Analytical letters. 2012 Jan 1;45(2-3):168-86.

23) Nahavandi S, Baratchi S, Soffe R, Tang SY, Nahavandi S, Mitchell A, Khoshmanesh K. Microfluidic platforms for biomarker analysis. Lab on a Chip. 2014;14(9):1496-514.

24) Martinez AW, Phillips ST, Whitesides GM, Carrilho E. Diagnostics for the developing world: microfluidic paper-based analytical devices.

25) Ellerbee AK, Phillips ST, Siegel AC, Mirica KA, Martinez AW, Striehl P, Jain N, Prentiss M, Whitesides GM. Quantifying colorimetric assays in paper-based microfluidic devices by measuring the transmission of light through paper. Analytical chemistry. 2009 Sep 1;81(20):8447-52.

26) Delaney JL, Hogan CF, Tian J, Shen W. Electrogenerated chemiluminescence detection in paper-based microfluidic sensors. Analytical chemistry. 2011 Jan 19;83(4):1300-6.

27) Cheng CM, Martinez AW, Gong J, Mace CR, Phillips ST, Carrilho E, Mirica KA, Whitesides GM. paper-based elisa. Angewandte Chemie International Edition. 2010 Jun 28;49(28):4771-4.

28) Bruzewicz DA, Reches M, Whitesides GM. Low-cost printing of poly (dimethylsiloxane) barriers to define microchannels in paper. Analytical chemistry. 2008 May 1;80(9):3387-92.

28) Demirel G, Babur E. Vapor-phase deposition of polymers as a simple and versatile technique to generate paper-based microfluidic platforms for bioassay applications. Analyst. 2014;139(10):2326-31.

29) N. R. Pollock, J. P. Rolland, S. Kumar, P. D. Beattie, S. Jain,F. Noubary, V. L. Wong, R. A. Pohlmann, U. S. Ryan and G. M. Whitesides. A paper-based multiplexed transaminase test for low-cost, point-of-care liver function testing . Sci. Transl. Med., 2012; 4(152):152ra 129.

30) Rivas L, de la Escosura-Muñiz A, Serrano L, Altet L, Francino O, Sánchez A, Merkoçi A. Triple lines gold nanoparticle-based lateral flow assay for enhanced and simultaneous detection of Leishmania DNA and endogenous control. Nano Research. 2015 Nov 1;8(11):3704-14.

31) Hartman MR, Ruiz RC, Hamada S, Xu C, Yancey KG, Yu Y, Han W, Luo D. Point-of-care nucleic acid detection using nanotechnology. Nanoscale. 2013;5(21):10141-54.

32) Connelly JT, Rolland JP, Whitesides GM. “Paper machine” for molecular diagnostics. Analytical chemistry. 2015 Jul 13;87(15):7595-601.

33) Cho EJ, Lee JW, Ellington AD. Applications of aptamers as sensors. Annual Review of Analytical Chemistry. 2009 Jul 19;2:241-64.

34) Berg JM, Tymoczko JL, Stryer L. Biochemistry (Loose-Leaf). Macmillan; 2008 Dec15.

35) Tang D, Sauceda JC, Lin Z, Ott S, Basova E, Goryacheva I, Biselli S, Lin J, Niessner R, Knopp D. Magnetic nanogold microspheres-based lateral-flow immunodipstick for rapid detection of aflatoxin B 2 in food. Biosensors and Bioelectronics. 2009 Oct 15;25(2):514-8.

36) San Park T, Li W, McCracken KE, Yoon JY. Smartphone quantifies Salmonella from paper microfluidics. Lab on a Chip. 2013;13(24):4832-40.

37) Ho JA, Wauchope RD. A strip liposome immunoassay for aflatoxin B1. Analytical chemistry. 2002 Apr 1;74(7):1493-6.

38) He Q, Ma C, Hu X, Chen H. Method for fabrication of paper-based microfluidic devices by alkylsilane self-assembling and UV/O3-patterning. Analytical chemistry. 2013 Jan 7;85(3):1327-31.

39) Wang J, Jin W, Zhang X, Hu C, Luo Q, Lin Y, Hu S. Rapid in situ detection of ultratrace 2, 4-dinitrotoluene solids by a sandwiched paper-like electrochemical sensor. Analytical chemistry. 2014 Aug 5;86(16):8383-90.

40) C. Parolo and A. Merkoçi, Paper-based nanobiosensors for diagnostics. Chem. Soc. Rev. 2013, 42(2), 450–457.

41) Zhang Y, Zuo P, Ye BC. A low-cost and simple paper-based microfluidic device for simultaneous multiplex determination of different types of chemical contaminants in food. Biosensors and Bioelectronics. 2015 Jun 15;68:14-9.

42) Chen Y, Wang Y, Liu L, Wu X, Xu L, Kuang H, Li A, Xu C. A gold immunochromatographic assay for the rapid and simultaneous detection of fifteen β-lactams. Nanoscale. 2015;7(39):16381-8.

43) Huang S, He Q, Xu S, Wang L. Polyaniline-based photothermal paper sensor for sensitive and selective detection of 2, 4, 6-trinitrotoluene. Analytical chemistry. 2015 May 7;87(10):5451-6.

44) Xu H, Mao X, Zeng Q, Wang S, Kawde AN, Liu G. Aptamer-functionalized gold

nanoparticles as probes in a dry-reagent strip biosensor for protein analysis. Analytical Chemistry. 2008 Dec 12;81(2):669-75.

45) Chamorro-Garcia A, de la Escosura-Muñiz A, Espinoza-Castañeda M, Rodriguez-Hernandez CJ, de Torres C, Merkoçi A. Detection of parathyroid hormone-like hormone in cancer cell cultures by gold nanoparticle-based lateral flow immunoassays. Nanomedicine: Nanotechnology, Biology and Medicine. 2016 Jan 31;12(1):53-61.

46) Zambre A, Chanda N, Prayaga S, Almudhafar R, Afrasiabi Z, Upendran A, Kannan R. Design and development of a field applicable gold nanosensor for the detection of luteinizing hormone. Analytical chemistry. 2012 Oct 16;84(21):9478-84.

47) Dou M, Dominguez DC, Li X, Sanchez J, Scott G. A versatile PDMS/paper hybrid microfluidic platform for sensitive infectious disease diagnosis. Analytical chemistry. 2014 Jul 24;86(15):7978-86.

48) Wallis RS, Kim P, Cole S, Hanna D, Andrade BB, Maeurer M, Schito M, Zumla A. Tuberculosis biomarkers discovery: developments, needs, and challenges. The Lancet infectious diseases. 2013 Apr 30;13(4):362-72.

49) Deiss F, Funes-Huacca ME, Bal J, Tjhung KF, Derda R. Antimicrobial susceptibility assays in paper-based portable culture devices. Lab on a Chip. 2014;14(1):167-71.

50) Morales-Narváez E, Naghdi T, Zor E, Merkoçi A. Photoluminescent lateral-flow immunoassay revealed by graphene oxide: highly sensitive paper-based pathogen detection. Analytical chemistry. 2015 Aug 4;87(16):8573-7.

51) Liu MQ, Tang L, Kong WH, Zhu ZR, Peng JS, Wang X, Yao ZZ, Schilling R, Zhou W. CD4+ T cell count, HIV-1 viral loads and demographic variables of newly identified patients with

HIV infection in Wuhan, China. Journal of medical virology. 2013 Oct 1;85(10):1687-91.

52) Takanashi S, Okame M, Shiota T, Takagi M, Yagyu F, Tung PG, Nishimura S, Katsumata N, Igarashi T, Okitsu S, Ushijima H. Development of a rapid immunochromatographic test for noroviruses genogroups I and II. Journal of virological methods. 2008 Mar 31;148(1):1-8.

53) Xia X, Xu Y, Zhao X, Li Q. Lateral flow immunoassay using europium chelate-loaded silica nanoparticles as labels. Clin Chem. 2009 Jan;55(1):179-82.

54) Corstjens P, Zuiderwijk M, Brink A, Li S, Feindt H, Niedbala RS, Tanke H. Use of up-converting phosphor reporters in lateral-flow assays to detect specific nucleic acid sequences: a rapid, sensitive DNA test to identify human papillomavirus type 16 infection. Clinical chemistry. 2001 Oct 1;47(10):1885-93.

55) Alkasir RS, Ornatska M, Andreescu S. Colorimetric paper bioassay for the detection of phenolic compounds. Analytical chemistry. 2012 Nov 5;84(22):9729-37.

56) Jayawardane BM, Wei S, McKelvie ID, Kolev SD. Microfluidic paper-based analytical device for the determination of nitrite and nitrate. Analytical chemistry. 2014 Jul 7;86(15):7274-9.

57) Pinrat O, Boonkitpatarakul K, Paisuwan W, Sukwattanasinitt M, Ajavakom A. Glucopyranosyl-1, 4-dihydropyridine as a new fluorescent chemosensor for selective detection of 2, 4, 6-trinitrophenol. Analyst. 2015;140(6):1886-93.

58) Li Z, Wang Y, Wang J, Tang Z, Pounds JG, Lin Y. Rapid and sensitive detection of protein biomarker using a portable fluorescence biosensor based on quantum dots and a lateral flow test strip. Analytical Chemistry. 2010 Jul 19;82(16):7008-14.

59) Sun G, Liu H, Zhang Y, Yu J, Yan M, Song X, He W. Gold nanorods-paper electrode based enzyme-free electrochemical immunoassay for prostate specific antigen using porous zinc oxide spheres–silver nanoparticles nanocomposites as labels. New Journal of Chemistry. 2015;39(8):6062-7.

60) Kumar S, Willander M, Sharma JG, Malhotra BD. A solution processed carbon nanotube modified conducting paper sensor for cancer detection. Journal of Materials Chemistry B. 2015;3(48):9305-14.

61) Wang S, Ge L, Song X, Yu J, Ge S, Huang J, Zeng F. based chemiluminescence ELISA: lab-on-paper based on chitosan modified paper device and wax-screen-printing. Biosensors and bioelectronics. 2012 Jan 15;31(1):212-8.

62) Choi DH, Lee SK, Oh YK, Bae BW, Lee SD, Kim S, Shin YB, Kim MG. A dual gold nanoparticle conjugate-based lateral flow assay (LFA) method for the analysis of troponin I. Biosensors and Bioelectronics. 2010 Apr 15;25(8):1999-2002.

63) Xu H, Mao X, Zeng Q, Wang S, Kawde AN, Liu G. Aptamer-functionalized gold nanoparticles as probes in a dry-reagent strip biosensor for protein analysis. Analytical Chemistry. 2008 Dec 12;81(2):669-75.

64) Gomes HI, Sales MG. Development of paper-based color test-strip for drug detection in aquatic environment: application to oxytetracycline. Biosensors and Bioelectronics. 2015 Mar 15;65:54-61.

65) San Park T, Li W, McCracken KE, Yoon JY. Smartphone quantifies Salmonella from paper microfluidics. Lab on a Chip. 2013;13(24):4832-40.

66) Ho JA, Wauchope RD. A strip liposome immunoassay for aflatoxin B1. Analytical

chemistry. 2002 Apr 1;74(7):1493-6.

67) Velu R, Frost N, DeRosa MC. Linkage inversion assembled nano-aptasensors (LIANAs) for turn-on fluorescence detection. Chemical Communications. 2015;51(76):14346-9.

68) López_Marzo AM, Pons J, Blake DA, Merkoçi A. High sensitive gold-nanoparticle based lateral flow immunodevice for Cd 2+ detection in drinking waters. Biosensors and Bioelectronics. 2013 Sep 15;47:190-8.

69) López Marzo AM, Pons J, Blake DA, Merkoçi A. All-integrated and highly sensitive paper based device with sample treatment platform for Cd2+ immunodetection in drinking/tap waters. Analytical chemistry. 2013 Mar 14;85(7):3532-8.

70) Nath P, Arun RK, Chanda N. Smart gold nanosensor for easy sensing of lead and copper ions in solution and using paper strips. Rsc Advances. 2015;5(84):69024-31.

71) Qi YX, Zhang M, Zhu A, Shi G. Terbium (III)/gold nanocluster conjugates: the development of a novel ratiometric fluorescent probe for mercury (II) and a paper-based visual sensor. Analyst. 2015;140(16):5656-61.

72) Wang L, Chen W, Ma W, Liu L, Ma W, Zhao Y, Zhu Y, Xu L, Kuang H, Xu C. Fluorescent strip sensor for rapid determination of toxins. Chemical Communications. 2011 Feb 7;47(5):1574-6.

73) Hu J, Wang S, Wang L, Li F, Pingguan-Murphy B, Lu TJ, Xu F. Advances in paper-based point-of-care diagnostics. Biosensors and Bioelectronics. 2014 Apr 15;54:585-97.

74) Monton MR, Forsberg EM, Brennan JD. Tailoring sol–gel-derived silica materials for optical biosensing. Chemistry of Materials. 2011 Nov 15;24(5):796-811.

75) Chamorro-Garcia A, de la Escosura-Muñiz A, Espinoza-Castañeda M, Rodriguez-

Hernandez CJ, de Torres C, Merkoçi A. Detection of parathyroid hormone-like hormone in cancer cell cultures by gold nanoparticle-based lateral flow immunoassays. Nanomedicine: Nanotechnology, Biology and Medicine. 2016 Jan 31;12(1):53-61.

76) Cunningham JC, Scida K, Kogan MR, Wang B, Ellington AD, Crooks RM. Paper diagnostic device for quantitative electrochemical detection of ricin at picomolar levels. Lab on a Chip. 2015;15(18):3707-15.

77) Ge L, Wang S, Song X, Ge S, Yu J. 3D Origami-based multifunction-integrated immunodevice: low-cost and multiplexed sandwich chemiluminescence immunoassay on microfluidic paper-based analytical device. Lab on a Chip. 2012;12(17):3150-8.

78) Yang X, Forouzan O, Brown TP, Shevkoplyas SS. Integrated separation of blood plasma from whole blood for microfluidic paper-based analytical devices. Lab on a Chip. 2012;12(2):274-80.

79) Khan MS, Thouas G, Shen W, Whyte G, Garnier G. Paper diagnostic for instantaneous blood typing. Analytical chemistry. 2010 Apr 23;82(10):4158-64.

80) Nilghaz A, Shen W. Low-cost blood plasma separation method using salt functionalized paper. Rsc Advances. 2015;5(66):53172-9.

81) Noiphung J, Songjaroen T, Dungchai W, Henry CS, Chailapakul O, Laiwattanapaisal W. Electrochemical detection of glucose from whole blood using paper-based microfluidic devices. Analytica chimica acta. 2013 Jul 25;788:39-45.

82)Bell J.M., Cameron F.K. The flow of liquids through capillary spaces. J.Phys. Chem.10, 1905, 658–674.

83) Schuchard D., Berg .J. Liquid transport in composite cellulose—super- absorbent fiber

networks.WoodFiberSci.1991 July ; 23(3),342–357.

84) Yager P, Edwards T, Fu E, Helton K, Nelson K, Tam MR, Weigl BH. Microfluidic diagnostic technologies for global public health. Nature. 2006 Jul 27;442(7101):412-8.

85) Fu E, Ramsey SA, Kauffman P, Lutz B, Yager P. Transport in two-dimensional paper networks. Microfluidics and nanofluidics. 2011 Jan 1;10(1):29-35.

86) Balu B, Berry AD, Hess DW, Breedveld V. Patterning of superhydrophobic paper to control the mobility of micro-liter drops for two-dimensional lab-on-paper applications. Lab Chip. 2009 Nov 7;9(21):3066-75.

87) Kauffman P, Fu E, Lutz B, Yager P. Visualization and measurement of flow in two-dimensional paper networks. Lab Chip. 2010 Oct 7;10(19):2614-7.

88) Lutz BR, Trinh P, Ball C, Fu E, Yager P. Two-dimensional paper networks: programmable fluidic disconnects for multi-step processes in shaped paper. Lab Chip. 2011 Dec 21;11(24):4274-8.

89) Kalish B, Tsutsui H. Patterned adhesive enables construction of nonplanar three-dimensional paper microfluidic circuits. Lab Chip. 2014 Nov 21;14(22):4354-61.

90) Han YL, Wang W, Hu J, Huang G, Wang S, Lee WG, Lu TJ, Xu F. Benchtop fabrication of three-dimensional reconfigurable microfluidic devices from paper–polymer composite. Lab on a Chip. 2013;13(24):4745-9.

91) Lewis GG, DiTucci MJ, Baker MS, Phillips ST. High throughput method for prototyping three-dimensional, paper-based microfluidic devices. Lab on a Chip. 2012;12(15):2630-3.

92) Liu H, Crooks RM. Three-dimensional paper microfluidic devices assembled using the principles of origami. Journal of the American Chemical Society. 2011 Oct

17;133(44):17564-6.

93) Li W, Li L, Ge S, Song X, Ge L, Yan M, Yu J. Multiplex electrochemical origami immunodevice based on cuboid silver-paper electrode and metal ions tagged nanoporous silver–chitosan. Biosensors and Bioelectronics. 2014 Jun 15;56:167-73.

94) Schilling KM, Jauregui D, Martinez AW. Paper and toner three-dimensional fluidic devices: programming fluid flow to improve point-of-care diagnostics. Lab Chip. 2013 Feb 21;13(4):628-31.

95) Zhong ZW, Wang ZP, Huang GX. Investigation of wax and paper materials for the fabrication of paper-based microfluidic devices. Microsystem technologies. 2012 May 1;18(5):649-59.

96) Hou L, Zhang W, Zhu L. Preparation of paper micro-fluidic devices used in bio-assay based on drop-on-demand wax droplet generation. Analytical Methods. 2014;6(3):878-85.

97) Cai L, Wu Y, Xu C, Chen Z. A simple paper-based microfluidic device for the determination of the total amino acid content in a tea leaf extract. Journal of Chemical Education. 2012 Dec 17;90(2):232-4.

98) Li X, Tian J, Garnier G, Shen W. Fabrication of paper-based microfluidic sensors by printing. Colloids Surf B Biointerfaces. 2010 Apr 1;76(2):564-70.

99) Olkkonen J, Lehtinen K, Erho T. Flexographically printed fluidic structures in paper. Analytical chemistry. 2010 Nov 23;82(24):10246-50.

100) Xia Y, Si J, Li Z. Fabrication techniques for microfluidic paper-based analytical devices and their applications for biological testing: A review. Biosensors and Bioelectronics.

2016 Mar 15;77:774-89.

101) Cai L, Xu C, Lin S, Luo J, Wu M, Yang F. A simple paper-based sensor fabricated by selective wet etching of silanized filter paper using a paper mask. Biomicrofluidics. 2014 Oct 13;8(5):056504.

102) Li L, Ma C, Kong Q, Li W, Zhang Y, Ge S, Yan M, Yu J. A 3D origami electrochemical immunodevice based on a Au@ Pd alloy nanoparticle-paper electrode for the detection of carcinoembryonic antigen. Journal of Materials Chemistry B. 2014;2(38):6669-74.

103) Apilux A, Siangproh W, Praphairaksit N, Chailapakul O. Simple and rapid colorimetric detection of Hg (II) by a paper-based device using silver nanoplates. Talanta. 2012 Aug 15;97:388-94.

104) West PW. Selective Spot Test for Copper. Industrial & Engineering Chemistry Analytical Edition. 1945 Nov;17(11):740-1.

105) Guan L, Cao R, Tian J, McLiesh H, Garnier G, Shen W. A preliminary study on the stabilization of blood typing antibodies sorbed into paper. Cellulose. 2014 Feb 1;21(1):717-27.

106) Hodgson KT, Berg JC. The effect of surfactants on wicking flow in fiber networks. Journal of colloid and interface science. 1988 Jan 1;121(1):22-31.

107) Roberts R, Senden T, Knackstedt M, Lyne MB. Spreading of aqueous liquids in unsized papers is by film flow.

108) Reed CM, Wilson N. The fundamentals of absorbency of fibres, textile structures and polymers. I. The rate of rise of a liquid in glass capillaries. Journal of physics D: Applied physics. 1993 Sep 14;26(9):1378.

109) Fries N, Dreyer M. An analytic solution of capillary rise restrained by gravity. Journal of colloid and interface science. 2008 Apr 1;320(1):259-63.

110) Reyssat M, Courbin L, Reyssat E, Stone HA. Imbibition in geometries with axial variations. Journal of Fluid Mechanics. 2008 Nov;615:335-44.

111) Xiao J, Stone HA, Attinger D. Source-like solution for radial imbibition into a homogeneous semi-infinite porous medium. Langmuir. 2012 Feb 21;28(9):4208-12.

112) Evans E, Gabriel EF, Coltro WK, Garcia CD. Rational selection of substrates to improve color intensity and uniformity on microfluidic paper-based analytical devices. Analyst. 2014;139(9):2127-32.

113) Stampfl J, Liska R, Sahli N, Belbachir M, Lutz PJ. www. mcp-journal. de. Macromol. Chem. Phys. 2005;206:1253-6.

114) Hanson Shepherd JN, Parker ST, Shepherd RF, Gillette MU, Lewis JA, Nuzzo RG. 3D microperiodic hydrogel scaffolds for robust neuronal cultures. Advanced functional materials. 2011 Jan 7;21(1):47-54.

115) Therriault D, White SR, Lewis JA. Chaotic mixing in three-dimensional microvascular networks fabricated by direct-write assembly. Nat Mater. 2003 Apr;2(4):265-71.

116) Ilievski F, Mazzeo AD, Shepherd RF, Chen X, Whitesides GM. Soft robotics for chemists. Angewandte Chemie. 2011 Feb 18;123(8):1930-5.

117) Symes MD, Kitson PJ, Yan J, Richmond CJ, Cooper GJ, Bowman RW, Vilbrandt T,Cronin L. Integrated 3D-printed reactionware for chemical synthesis and analysis.Nat Chem. 2012 Apr 15;4(5):349-54.

118) Kitson PJ, Rosnes MH, Sans V, Dragone V, Cronin L. Configurable 3D-Printed millifluidic

and microfluidic ‘lab on a chip’reactionware devices. Lab on a Chip. 2012;12(18):3267-71.

119) Wang Z, Martin N, Hini D, Mills B, Kim K. Rapid Fabrication of Multilayer Microfluidic Devices Using the Liquid Crystal Display-Based Stereolithography 3D Printing System. 3D Printing and Additive Manufacturing. 2017 Sep 1;4(3):156-64.

120) Salentijn GI, Oomen PE, Grajewski M, Verpoorte E. Fused Deposition Modeling 3D Printing for (Bio) analytical Device Fabrication: Procedures, Materials, and Applications. Analytical chemistry. 2017 Jun 19;89(13):7053-61.

121) Chen C, Mehl BT, Munshi AS, Townsend AD, Spence DM, Martin RS. 3D-printed microfluidic devices: fabrication, advantages and limitations—a mini review. Analytical Methods. 2016;8(31):6005-12.

122) He Y, Gao Q, Wu WB, Nie J, Fu JZ. 3D Printed Paper-Based Microfluidic Analytical Devices. Micromachines. 2016 Jun 28;7(7):108.

123) Christensen K, Huang Y. Study of Layer Formation During Droplet-Based Three-Dimensional Printing of Gel Structures. Journal of Manufacturing Science and Engineering. 2017 Sep 1;139(9):091009.

124) He Y, Wildman RD, Tuck CJ, Christie SD, Edmondson S. An investigation of the behavior of solvent based polycaprolactone ink for material jetting. Scientific reports. 2016 Feb 12;6:20852.

125) Ramanath HS, Chua CK, Leong KF, Shah KD. Melt flow behaviour of poly-ε-caprolactone in fused deposition modelling. Journal of Materials Science: Materials in Medicine. 2008 Jul 1;19(7):2541-50.

126)Jiang CP, Huang JR, Hsieh MF. Fabrication of synthesized PCL-PEG-PCL tissue engineering scaffolds using an air pressure-aided deposition system. Rapid Prototyping Journal. 2011 Jun 14;17(4):288-97.

127)Williams JM, Adewunmi A, Schek RM, Flanagan CL, Krebsbach PH, Feinberg SE, Hollister SJ, Das S. Bone tissue engineering using polycaprolactone scaffolds fabricated via selective laser sintering. Biomaterials. 2005 Aug 31;26(23):4817-27.

128)Eshraghi S, Das S. Mechanical and microstructural properties of polycaprolactone scaffolds with one-dimensional, two-dimensional, and three-dimensional orthogonally oriented porous architectures produced by selective laser sintering. Acta biomaterialia. 2010 Jul 31;6(7):2467-76.

129)An J, Teoh JE, Suntornnond R, Chua CK. Design and 3D printing of scaffolds and tissues. Engineering. 2015 Jun 30;1(2):261-8.

130)Abbas A, Linman MJ, Cheng Q. New trends in instrumental design for surface plasmon resonance-based biosensors. Biosens Bioelectron. 2011 Jan 15;26(5):1815-24.

131)Davaji B, Lee CH. A paper-based calorimetric microfluidics platform for bio-chemical sensing. Biosens Bioelectron. 2014 Sep 15;59:120-6.

132)Gáspár A, Bácsi I. Forced flow paper chromatography: A simple tool for separations in short time. Microchemical Journal. 2009 May 31;92(1):83-6.

133)Zhong ZW, Wang ZP, Huang GX. Investigation of wax and paper materials for the fabrication of paper-based microfluidic devices. Microsystem technologies. 2012 May 1;18(5):649-59.

135)Zhou M, Yang M, Zhou F. Paper based colorimetric biosensing platform utilizing cross-

linked siloxane as probe. Biosensors and Bioelectronics. 2014 May 15;55:39-43..

136) Lee S, Oncescu V, Mancuso M, Mehta S, Erickson D. A smartphone platform for the quantification of vitamin D levels. Lab on a Chip. 2014;14(8):1437-42.

137) Koesdjojo MT, Wu Y, Boonloed A, Dunfield EM, Remcho VT. Low-cost, high-speed identification of counterfeit antimalarial drugs on paper. Talanta. 2014 Dec 1;130:122-7.

138) Mani R. Science of measurements in wound healing. Wound Repair and Regeneration. 1999 Sep 1;7(5):330-4.

139) Prompers L, Huijberts M, Schaper N, Apelqvist J, Bakker K, Edmonds M, Holstein P, Jude E, Jirkovska A, Mauricio D, Piaggesi A. Resource utilisation and costs associated with the treatment of diabetic foot ulcers. Prospective data from the Eurodiale Study. Diabetologia. 2008 Oct 1;51(10):1826..

140) Armstrong DG, Lipsky BA. Diabetic foot infections: stepwise medical and surgical management. International Wound Journal. 2004 Jun 1;1(2):123-32.

141) Kim J, Moon MW, Lee KR, Mahadevan L, Kim HY. Hydrodynamics of writing with ink. Physical review letters. 2011 Dec 20;107(26):264501.

142) http://www.dataphysics.de

143) Shukla V, Kandeepan G, Vishnuraj MR, Soni A. Anthocyanins Based Indicator Sensor for Intelligent Packaging Application. Agricultural Research. 2016 Jun 1;5(2):205-9.